The Environmental Pollutant Tributyltin Chloride Disrupts the Hypothalamic-Pituitary-Adrenal Axis at Different Levels in Female Rats

Eduardo Merlo, Priscila L. Podratz, Gabriela C. Sena, Julia F. P. de Araújo, Leandro C. F. Lima, Izabela S. S. Alves, Letícia N. Gama-de-Souza, Renan Pelição, Lívia C. M. Rodrigues, Poliane A. A. Brandão, Maria T. W. D. Carneiro, Rita G. W. Pires, Cristina Martins-Silva, Tamara A. Alarcon, Leandro Miranda-Alves, Ian V. Silva, and Jones B. Graceli

Department of Morphology (E.M., P.L.P., G.C.S., J.F.P.d.A., I.S.S.A., L.N.G.-d.S., I.V.S., J.B.G.), Federal University of Espírito Santo, Vitória ES, 29040090 Brazil; Department of Biophysics and Physiology (L.C.F.L.), Federal University of Minas Gerais, Vitória ES, 29040090 Brazil; Department of Physiological Sciences (R.P., L.C.M.R., R.G.W.P., C.M.-S., T.A.A.), Federal University of Espírito Santo, Vitória ES, 29040090 Brazil; Department of Chemistry (P.A.A.B., M.T.W.D.C.), Federal University of Espírito Santo, Vitória ES, 29040090 Brazil; Experimental Endocrinology Research Group (L.M.-A.), Institute of Biomedical Sciences, Federal University of Rio de Janeiro, Vitória ES, 29040090 Brazil; and Postgraduate Program in Endocrinology (L.M.-A.), School of Medicine, Federal University of Rio de Janeiro, Vitória ES, 29040090 Brazil

Tributyltin chloride (TBT) is an environmental contaminant that is used as a biocide in antifouling paints. TBT has been shown to induce endocrine-disrupting effects. However, studies evaluating the effects of TBT on the hypothalamus-pituitary-adrenal (HPA) axis are especially rare. The current study demonstrates that exposure to TBT is critically responsible for the improper function of the mammalian HPA axis as well as the development of abnormal morphophysiology in the pituitary and adrenal glands. Female rats were treated with TBT, and their HPA axis morphophysiology was assessed. High CRH and low ACTH expression and high plasma corticosterone levels were detected in TBT rats. In addition, TBT leads to an increased in the inducible nitric oxide synthase protein expression in the hypothalamus of TBT rats. Morphophysiological abnormalities, including increases in inflammation, a disrupted cellular redox balance, apoptosis, and collagen deposition in the pituitary and adrenal glands, were observed in TBT rats. Increases in adiposity and peroxisome proliferator-activated receptor-γ protein expression in the adrenal gland were observed in TBT rats. Together, these data provide in vivo evidence that TBT leads to functional dissociation between CRH, ACTH, and costicosterone, which could be associated an inflammation and increased of inducible nitric oxide synthase expression in hypothalamus. Thus, TBT exerts toxic effects at different levels on the HPA axis function. **(*Endocrinology* 157: 2978–2995, 2016)**

The hypothalamus-pituitary-adrenal (HPA) axis is one of the most important neuroendocrine axes, and it plays a key role in stress processes, which is critical for normal physiology (1, 2). The hypothalamic CRH plays a pivotal role in regulating the cascade of hormonal events that is necessary for adrenal maturation. CRH is synthesized and released by parvocellular neurons and stimulates the production and secretion of ACHT in corticotrophs

ISSN Print 0013-7227 ISSN Online 1945-7170
Printed in USA

Received October 22, 2015. Accepted May 31, 2016.
First Published Online June 7, 2016

For News & Views see page 2996

Abbreviations: ADX, adrenalectomy; CON, control; CYP11B, steroid 11β-hydroxylase; D, days; DHE, dihydroethidium; EDC, endocrine-disrupting chemical; GAPDH, glyceraldehyde-3-phosphate dehydrogenase; H&E, hematoxylin and eosin; HPA, hypothalamus-pituitary-adrenal; iNOS, inducible nitric oxide synthase; MPO, myeloperoxidase; NAG, n-acetyl-β-d-glucosaminidase; OS, oxidative stress development process; OT, organotin; PPAR, peroxisome proliferator-activated receptor; qPCR, quantitative PCR; StAR, steroidogenic acute regulatory protein; TBT, tributyltin chloride; TBTO, bis (trin-butyltin) oxide; TEM, transmission electron microscopy; TM, trichrome; UFES, Federal University of Espírito Santo.

(3–5). ACTH acts on melanocortin-2 receptors to stimulate normal adrenal function (6).

The adrenal contains 2 regions, the adrenal cortex and medulla (7). The adrenal cortex is divided into 3 distinct zones, each of which has important functions (6–8). The zona glomerulosa secretes aldosterone, which acts as a modulator of electrolyte balance in the body. Glucocorticoids are secreted primarily from the zona fasciculate, which modulates metabolic and immune functions. The zona reticularis participates in androgen production, except in rodents (8–11). In addition, the adrenal medulla secretes catecholamines into the bloodstream (8, 10).

Recent studies have reported that HPA axis function is affected by environmental factors (12, 13). Rosol et al (14) and Harvey (15) reported that environment factors, especially the presence of endocrine-disrupting chemicals (EDCs), can alter HPA axis function. EDCs can affect the modulation of HPA axis, increase the levels of CYP family enzymes, and alter the capacity for the uptake and storage of lipophilic agents (14–16). Organotins (OTs), such as tributyltin chloride (TBT), have been identified as EDCs (17–21). TBT is an industrial contaminant that was once used as a naval antifouling agent (22, 23). TBT is lipophilic and tends to accumulate in seafood; consequently, human exposure occurs mainly through TBT-contaminated seafood (24, 25). OTs are detected in human blood at levels ranging from 64 to 155 ng/mL (260- to 610-ng/g dry weight), leading to TBT tissue accumulation and dysfunction (24). TBT exposure can lead to alterations in neural, reproductive, immune, and metabolic functions in both in vivo and in vitro models, suppressing immune responses and increasing adiposity (26–32). Studies have support the key roles of inflammatory mediators and obesity in the abnormal HPA axis function (33–35).

Because the discovery of TBT, few studies have evaluated the effects of TBT on HPA axis function, and its effects on HPA axis remain unclear (36, 37). In order to test the hypothesis that TBT will lead to abnormalities in HPA axis, we analyzed the key indicators of HPA axis competence in female rats, such as morphology, CRH and ACTH expression, inflammation and apoptosis, corticosterone hormone levels, and markers of oxidative stress development process (OS). The identification of the toxic signaling mechanisms affected by TBT in the HPA axis greatly contributes to our continuously evolving understanding of the HPA axis.

Materials and Methods

Chemicals

The chemical used was TBT (96%; Sigma), which was dissolved in a 0.4% ethanol based on the protocols in previous studies performed in our laboratory (30, 37, 38). The reagent used was of analytical grade.

Experimental animals

Adult female Wistar rats (12 wk old), were maintained under controlled temperature between 23°C–25°C with a 12-hour light, 12-hour dark cycle. Rat chow and filtered tap water were provided at libitum. All protocols were approved by the Ethics Committee of Animals of the Federal University of Espírito Santo (UFES) (106/2011). In this study, the total number of animals used was 138 rats. The rats were divided into 3 groups: control (CON) (n = 22) rats were treated daily with vehicle (0.4% ethanol); TBT15 (TBT15Days [D], n = 22) and TBT30 (TBT30D, n = 22) rats were treated daily with TBT (100 ng/kg · d) for 15 and 30 days, respectively, by gavage. All animals were anesthetized using ketamine and xylazine (90 and 4.5 mg/kg, ip) before euthanasia, and wet organs were weighed. The doses and routes of exposure were chosen based on protocols previously reported by us (38–40) and others (41) to increase the serum tin levels (31). Oral exposure to TBT in female rats was chosen, so we could compare the current findings with our previous work demonstrating metabolic toxicity (31). In addition, the TBT dose used in the current study (100 ng/kg) was approximately 3 times lower than the tolerable daily intake level of 300 ng/kg for humans established by the United States Environmental Protection Agency (42).

Tissue preparation

The adrenals and pituitary were removed, their wet weights were obtained, and they were fixed in PBS-formalin (4%) (pH 7.4), for 24–48 hours at room temperature. Paraffin-embedded organs were sectioned into 7-μm-thick slices and stained with hematoxylin and eosin (H&E) (43, 44). The anterior pituitary and adrenal gland are referred to as the pituitary and adrenal, respectively, throughout this study. Tissue processing and microscopic analyses were performed at the Laboratory of Cellular Ultrastructure Carlos Antonio Redins, UFES.

Histomorphometry

The histomorphometry image analysis system was composed of a digital camera (Evolution, Media Cybernetics, Inc) coupled to a light microscope (Olympus AX70; Olympus). High-resolution images (2048 × 1536 pixels) were captured using Carl Zeiss AxioVision Rel. 4.8. Photomicrographs were obtained using a ×10 objective, and the cortex and medulla of the adrenal area were assessed using the area measure tool of Axio Vision Rel. 4.8 (45).

Mast cell assessment

Pituitary and adrenal sections were stained with Alcian Blue according to a standard protocol (Sigma-Aldrich Co, LLC). Each of the 7-μm sections was used to obtain 20 photomicrographs (×40 objective). The number of positively stained cells (ie, cells containing purple cytoplasmic granules) within the tissue was evaluated. The areas to be analyzed were randomly selected, with the exception that fields containing medium-sized blood vessels were carefully avoided. The number of positively stained cells was then expressed per unit area (mm^2), as described in our previous studies (31, 40).

Collagen density surface assessment

TBT exposure was associated with tissue injury that could be repaired with collagen deposition (38, 39, 41). For this reason, we evaluated collagen deposition in the pituitary and adrenal glands after TBT exposure. Masson's trichrome (TM)-stained sections were used to obtain 15 photomicrographs of the pituitary and adrenal using a ×20 objective. The areas of the pituitary were randomly selected, and the areas containing the neurohypophysis were carefully avoided (N). The random fields from each well were photographed under phase contrast and analyzed using ImageJ. The images were converted into high-contrast black and white images to visualize stained collagen fibers. The results represent the percentage of collagen deposited in the total cortex of the adrenal and pituitary (39).

Tissue extraction and assessment of myeloperoxidase (MPO) and n-acetyl-β-d-glucosaminidase (NAG) activity

The infiltration of mononuclear cells into the pituitary and adrenal was quantified by measuring the level of the lysosomal enzyme NAG, which is present at high levels in activated macrophages (46). The pituitary and adrenal were homogenized in 0.9% saline solution containing 0.1% vol/vol Triton X-100 (Promega) and then centrifuged. A sample of the resulting supernatant was incubated for 10 minutes with 100 mL of p-nitrophenyl-n-acetyl-β-d-glucosaminide (Sigma-Aldrich Co, LLC) that was prepared in citrate/phosphate buffer (0.1M citric acid and 0.1M Na_2HPO_4; pH 4.5) to yield a final concentration of 2.24mM. The reaction was terminated by adding 100 mL of 0.2M glycine buffer (pH 10.6). Hydrolysis of the substrate was determined by measuring absorption at 400 nm. The results are expressed as nmol/μg of protein.

The number of neutrophils in the pituitary and adrenal was measured by assaying MPO activity, as previously described (47). The pituitary and adrenal were weighed, homogenized in pH 4.7 buffer (0.1M NaCl, 0.02M $NaPO_4$, and 0.015M NaEDTA), and centrifuged. The pellets were then resuspended in 0.05M $NaPO_4$ buffer (pH 5.4) containing 0.5% hexadecyltrimethylammonium bromide, followed by 3 freeze-thaw cycles using $N_{2(l)}$. MPO activity in the supernatant samples was assayed by measuring the change in absorbance (OD) at 450 nm using tetramethylbenzidine (1.6mM) and H_2O_2 (0.3mM). The reaction was terminated by adding 50 mL of H_2SO_4 (4M). The results are expressed as a change in OD/μg of protein.

RT-quantitative PCR (qPCR)

Real-time qPCR was performed to determine the expression levels of CRH mRNA in the hypothalamus and steroidogenic acute regulatory protein (StAR) mRNA in the adrenals in the CON and TBT-treated rats. Animals were decapitated and the brains were dissected previously and stored at −80°C until measurement following the protocol described by Quennell et al (48). Briefly, the whole hypothalamus was dissected along the following boundaries: laterally 2 mm either side of the third ventricle from the optic chiasm to the posterior border of the mammillary bodies, and the thalamus dorsally.

RNA was isolated from these tissues using TRI Reagent RNA Isolation Reagent (Sigma-Aldrich), according to the protocol provided by the supplier. One microgram of RNA was reverse transcribed using an iScript cDNA kit (Bio-Rad Laboratories). Real-time qPCR was performed in triplicate using the SYBR Green Master Mix (Bio-Rad Laboratories) and the CFX96 qPCR machine (Bio-Rad Laboratories). The primers used to amplify CRH were sense primer 5′-TGAGGGAAGTCTTGGAAATGG-3′, and antisense primer, 5′-CAGAGCTGCAGTATGGTA-CAG-3′. The primers used to amplify StAR were sense primer 5′-AAGGTTTCATAGATA CCTGTCCCTTAA-3′, and antisense primer, 5′-AGGAAAACAGAACTGAGGCTTAGAATA-3′.β-actin RNA was used as an internal control for cDNA input, sense primer 5′-ACA ACC TTC TTG CAG CTC CTC-3′, and antisense primer 5′-GCC GTG TTC AAT GGG GTA CT-3′. The relative quantification of mRNA expression was analyzed via the $2^{-\Delta\Delta Ct}$ threshold cycle method (49).

Hormonal assays

To measure basal levels of ACTH and corticosterone, plasma samples were obtained from animals that had been euthanized by decapitation without anesthesia between 8 and 9 AM (50). ACTH levels were measured using an ELISA kit assay (2244 EIA-3647; DRG Instruments GmbH) on an ELx808 Absorbance Microplate Reader (BioTek Instruments, Inc). A standard curve was generated using 5-fold serial dilutions of the hormone reference provided by The DRG Instruments GmbH. Low- and high-quality CONs were run on each assay to assess coefficient of variation values. The assay detection limit for ACTH was 0.22 pg/mL. The intraassay coefficient of variation for each assay was between 2.3% and 6.7%. The interassay coefficient of variation for each assay was between 6.9% and 7.1%. Corticosterone levels were measured using a RIA kit (07-120102 ICN corticosterone RIA; MP Biomedical) with a detection limit of 7.7 ng/mL. The intraassay coefficient of variation for each assay was between 4.4% and 10.3%. The interassay coefficient of variation for each assay was between 6.5% and 7.1%.

Total cholesterol assessment

To evaluate serum and adrenal total cholesterol, serum and adrenal samples were obtained, and the cholesterol levels were measured using colorimetric kits according to the manufacturer's directions (Bioclin) (31, 51).

Lipid deposition assessment

Adrenals were dissected, embedded in Tissue-Tek CRYO-OCT (Fisher Scientific), frozen and cross-sectioned to at a thickness of 7 μm using a cryostat (Jung CM1800; Leica). For each animal, the adrenals were mounted on gelatin-coated slides and stained using Oil Red O (Sigma-Aldrich). Lipid droplets were quantified using an Olympus microscope that was attached to an Evolution video camera and an image analysis system (ImageJ, Public Domain). The lipid droplet area per section is expressed as a percentage of the area of adrenal cortex that was analyzed (31).

Transmission electron microscopy (TEM)

Adrenal samples were prefixed in 2% glutaraldehyde fixative (in pH 7.4 PBS for 10 h at 4°C) and postfixed in 1% osmium tetroxide fixative (in pH 7.4 PBS for 30 min at 4°C). Subsequently, samples were dehydrated in via graded acetone series and embedded in epon. Ultrathin sections, 50–60 nm, were cut with a Power tomex microtome (RMC product). The sections were mounted on a copper grid and stained with uranylacetate

and lead citrate. The tissue sections were examined using a JEOL (JEM-1400) EM (44).

Protein extraction and immunoblotting

The hypothalamus, pituitary and adrenal were homogenized in lysis buffer, and total protein was obtained (31). Briefly, proteins were transferred to nitrocellulose membranes in tris-glycine buffer (Bio-Rad Laboratories). The membranes were incubated overnight with 5% blotting-grade blocker containing nonfat dry milk in tris-buffered saline plus 0.1% Tween 20 solution and specific antibodies (Bio-Rad Laboratories). The primary antibodies were anti-caspase-3 (sc7148, 1:500; SCBT, Inc), anti-ACTH (AB902, 1:800; Chemicon International), anti-β-actin (sc-130657, 1:1000; SCBT, Inc), antiperoxisome proliferator-activated receptor (PPAR)γ (sc-7273, 1:500; SCBT, Inc), anti-$CYP_{11B}1$ (sc28205, 1:500; SCBT, Inc), anti-inducible nitric oxide synthase (iNOS) (BD-610329; BD Transduction Laboratories), and antiglyceraldehyde-3-phosphate dehydrogenase (GAPDH) (sc25778, 1:1000; SCBT, Inc). Goat antirabbit IgG-alkaline phosphatase conjugate (A3687, 1:1000; Sigma-Aldrich) was used as a secondary antibody for all blotting assays unless noted. PPARγ and iNOS proteins were detected using a secondary antimouse IgG alkaline phosphatase conjugate (A3562, 1:1000; Sigma-Aldrich Co, LLC). The blots for iNOS, ACTH, $CYP_{11B}1/2$, PPARγ, and caspase-3, and their respective β-actin or GAPDH CONs were visualized using a color development reaction containing nitroblue tetrazolium chloride and 5-bromo-4-chloro-3-indolylphosphate *p*-toluidine salt (sc24981; SCBT, Inc). The iNOS, ACTH, $CYP_{11B}1/2$, PPARγ, caspase-3, GAPDH, and β-actin bands were analyzed by densitometry using ImageJ software. Relative expression levels were normalized by dividing the values for the protein of interest by the corresponding internal control values.

Superoxide anion assessment

To detect superoxide anion (O_2^-) levels, cryosections (8 μm) of adrenal and pituitary tissues embedded in OCT were allowed to thaw and were then incubated with the O_2^--sensitive fluorescent dye dihydroethidium (DHE) at 37°C for 30 minutes in the dark (39). Images were obtained using a Leica microscope with fluorescence detected at 585 nm (DM 2500). The signal intensity, indicating O_2^- production, was analyzed in the area of interest in 20 sections through the organ by a blinded researcher. Processing and microscopic analyses were performed at the Laboratory of Molecular Histology and Immunohistochemistry, UFES. The O_2^- production level indicates OS (LHMI).

Restraint stress assessment

Restraint stress was performed between 8 and 9 AM and lasted for 30 minutes. Other set of rats from CON, TBT15D, and TBT30D groups (n = 20 per group) were placed individually into horizontal perforated Plexiglas tubes with partial movement allowed (52). Blood samples were taken immediately before the stress procedure to estimate basal ACTH levels (0 time point, n = 5 per group). Blood samples were also drawn at 15 (n = 5 per group) and 30 minutes (n = 5 per group) during the stress procedure and 30 minutes after the termination of the stress procedure (n = 5 per group). To measure the ACTH levels, plasma samples were obtained from animals submitted to the stress procedure; animals were euthanized by decapitation without anesthesia (50). For CRH mRNA analysis by RT-qPCR in the hypothalamus, the brains were obtained from rats submitted to 30 minutes of stress; animals were decapitated and dissected following the protocol described by Quennell et al (48).

Evaluation of negative feedback by glucocorticoids

To evaluate the negative feedback by glucocorticoids, other set of 12-week-old female rats were anesthetized with ketamine-xylazine, and a bilateral adrenalectomy (ADX) (n = 12) was performed via a dorsal incision (53). Immediately after surgery, all rats were injected with penicillin (0.2 mL, 300 000 IU im) and buprenorphine (0.05 mg/kg, ip) prophylactically for postsurgical infection and pain. To maintain the electrolyte balance, ADX rats were provided with 0.9% saline in drinking water for the remainder of the experiment. After a 7-day recovery period, the ADX rats were underwent the treatment performed in the CON, TBT15D, and TBT30D groups described above (n = 4 per group). Blood was collected by decapitation without anesthesia, and plasma samples were collected and stored at −80°C until ACTH was measured as described above. In addition, hypothalamic CRH mRNA analysis was performed using RT-qPCR as described above.

Statistical analysis

All data are reported as the mean ± SEM. The normality test used to evaluate the data was the D'Agostino and Pearson omnibus. Comparisons between groups were performed using one- and two-way ANOVA for Gaussian data (Tukey's multiple comparison test). In addition, for non-Gaussian data, we used a Kruskal-Wallis test followed by Dunn's multiple comparisons. $P \leq .05$ was regarded as statistically significant.

Results

Abnormal pituitary morphology in TBT rats

To characterize the effects of TBT exposure, pituitary anatomy and histology were evaluated (Figure 1). A small increase in the size of the pituitary in TBT-exposed rats was observed in their anatomy (n = 5) (Figure 1A). An increase of between 14% and 37% was observed in pituitary weight in TBT15D and TBT30D rats, respectively, and the values in TBT30D rats were significantly different only when compared with CON rats (CON: 11.08 ± 0.74; TBT15D: 12.64 ± 0.80; TBT30D: 15.12 ± 1.40 mg, n = 5; $P \leq .05$) (Figure 1B). In pituitary histology, CON rats displayed all types of chromophil cells (acidophil and basophil) and normal capillaries interspersed the cell cords (n = 5) (Figure 1, C and C1). The presence of chromophobe cells is indicated by an arrowhead. The pituitary in both groups of TBT rats exhibited morphological abnormalities, such as a pituitary hyperplasia, mitosis (arrow, Figure 1, D1, E1), and disorganization of the cell cords (n = 5) (Figure 1, D, D1, E, and E1).

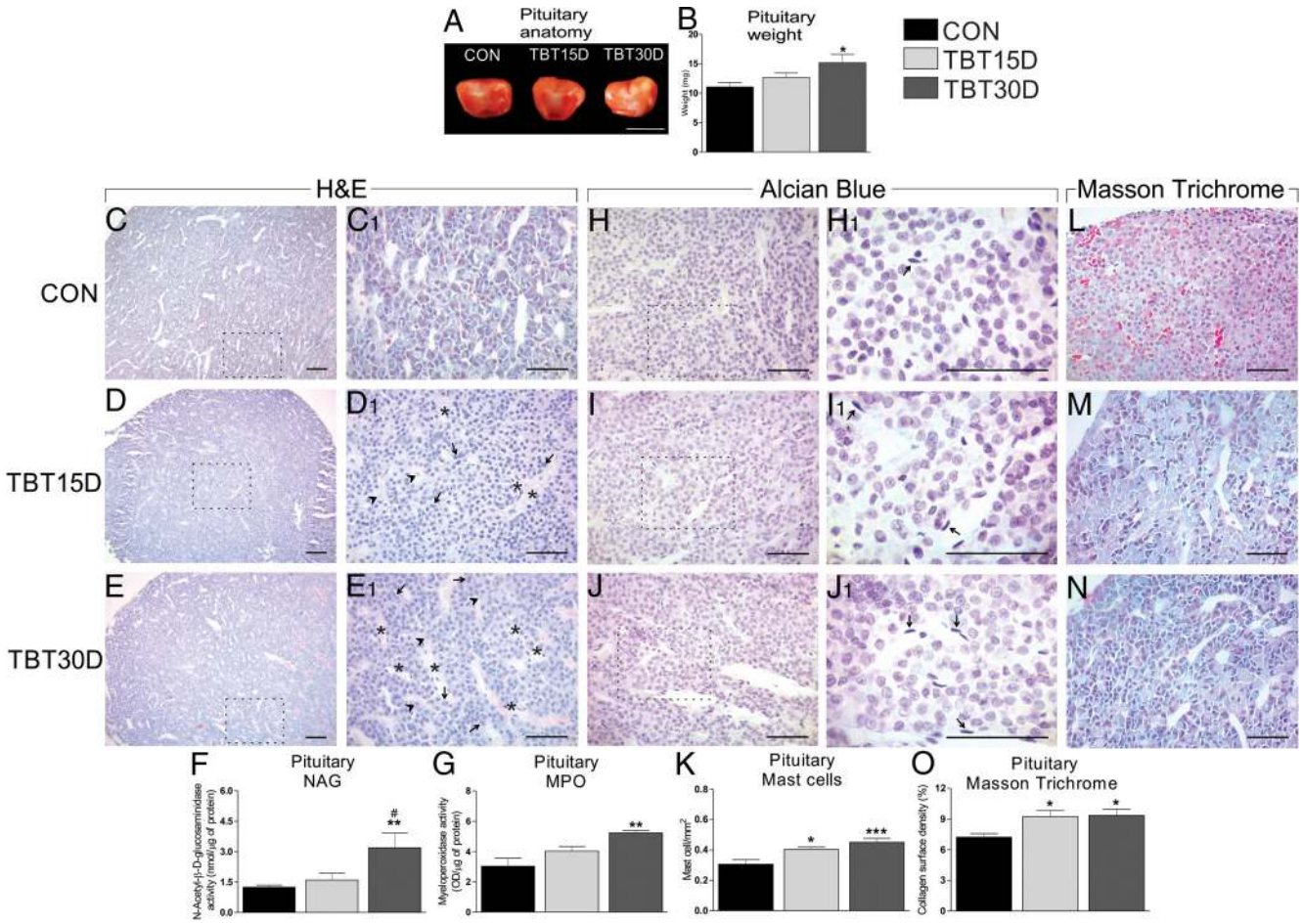

Figure 1. Anatomy and histomorphology of the pituitary in female rats. A, Pituitaries from CON, TBT15D, and TBT30D rats showing a small increase in the pituitaries of TBT30D rats. Scale bar, 300 mm (n = 5). B, Increased weight of the pituitary in TBT30D rats (n = 5). Representative sections from (C and C1) CON, (D and D1) TBT15D, and (E and E1) TBT30D pituitaries that were stained with H&E (n = 5). Chromophobe cell: arrowhead; mitosis, arrow; inflammatory cell, asterisk. F, Increased NAG activity in a pituitary from a TBT30D rat (n = 5). G, Increased MPO activity in a pituitary from a TBT30D rat (n = 5). Representative mast cells sections from (H and H1) CON, (I and I1) TBT15D, and (J and J1) TBT30D pituitaries that were stained with Alcian Blue (arrow) (n = 5). K, Increased mast cells in pituitaries from TBT15D and TBT30D rats (n = 5). Representative collagen-stained sections in (L) CON, (M) TBT15D, and (N) TBT30D pituitaries that were stained with Masson's TM (n = 5). O, Increased collagen surface density in pituitaries from TBT15D and TBT30D rats (n = 5). Scale bar, 50 μm. One-way ANOVA, Tukey's multiple comparison test; *, $P \leq .05$; **, $P \leq .01$; **, $P \leq .001$ vs CON; #, $P \leq .05$ vs TBT15D.

Inflammation was higher in the pituitaries of TBT rats

Intensely stained capillaries surrounded and infiltrated by inflammatory cells between pituitary acini were observed in the pituitaries from both TBT groups (asterisk). Pituitary NAG activity was higher in TBT_{30D} rats compared with CON rats (CON: 1.25 ± 0.10; TBT15D: 1.60 ± 0.35; TBT30D: 3.19 ± 0.72 nmol/μg, n = 5; $P \leq .05$) (Figure 1F), and it was also higher when we compared TBT30D with TBT15D rats. Pituitary NAG activity was similar in the CON and TBT15D rats ($P > .05$). An increase in pituitary MPO activity was observed in TBT30D rats compared with CON rats (CON: 3.03 ± 0.53; TBT15D: 4.02 ± 0.31; TBT30D: 5.23 ± 0.16 OD/μg, n = 5; $P \leq .01$) (Figure 1G). Pituitary MPO activity was similar between CON and TBT15D rats and, TBT15D, and TBT30D rats ($P \geq .05$). In addition, pituitary mast cells were observed in CON, TBT15D, and TBT30D rats using the Alcian Blue staining (Figure 1, H, H1, I, I1, J, and J1). However, a large number of mast cell was observed in the pituitary of both groups of TBT rats. The number of pituitary mast cells was higher in both groups of TBT rats compared with the CON rats (CON: 0.31 ± 0.03; TBT15D: 0.40 ± 0.02; TBT30D: 0.45 ± 0.02 mast cells/mm^2, n = 5; $P \leq .05$) (Figure 1, H, H1, I, I1, J, J1, and K, arrow). No significant difference in pituitary mast cell number was observed in TBT15D and TBT30D rats ($P \geq .05$).

Collagen deposition was higher in the pituitary of TBT rats

Furthermore, an assessment of pituitary collagen deposition was also performed in CON, TBT15D, and

TBT30D rats using TM staining (Figure 1, L–N). The collagen surface density in both groups of TBT rats was higher than the density in CON rats (CON: 7.23 ± 0.34; TBT15D: 9.23 ± 0.64; TBT30D: 9.37 ± 0.62%, n = 5; $P \leq .05$) (Figure 1O). No significant difference in collagen surface density was observed in the pituitary between TBT15D and TBT30D rats ($P \geq .05$).

Hypothalamic CRH mRNA expression in TBT rats

CRH mRNA was evaluated in samples of hypothalamic tissue from the CON group and both groups of TBT-treated rats (Figure 2). CRH mRNA was approximately 70%–90% higher in hypothalamic tissue from TBT-treated rats compared with tissue from CON rats (n = 4, $P \leq .05$) (Figure 2A). No significant differences in hypothalamic CRH mRNA were observed between TBT15D and TBT30D rats ($P \geq .05$).

Hypothalamic iNOS expression in TBT rats

iNOS protein expression was evaluated in the hypothalamus of CON rats and both groups of TBT rats. An increase in iNOS protein expression was observed in TBT30D rats compared with CON rats (CON: 1.00 ± 0.04; TBT15D: 1.11 ± 0.09; TBT30D: 1.28 ± 0.07, n = 5; $P \leq .05$) (Figure 2B). No significant differences in hypothalamic iNOS protein expression were detected between the CON rats and TBT15D rats or between TBT15D and TBT30D rats ($P \geq .05$).

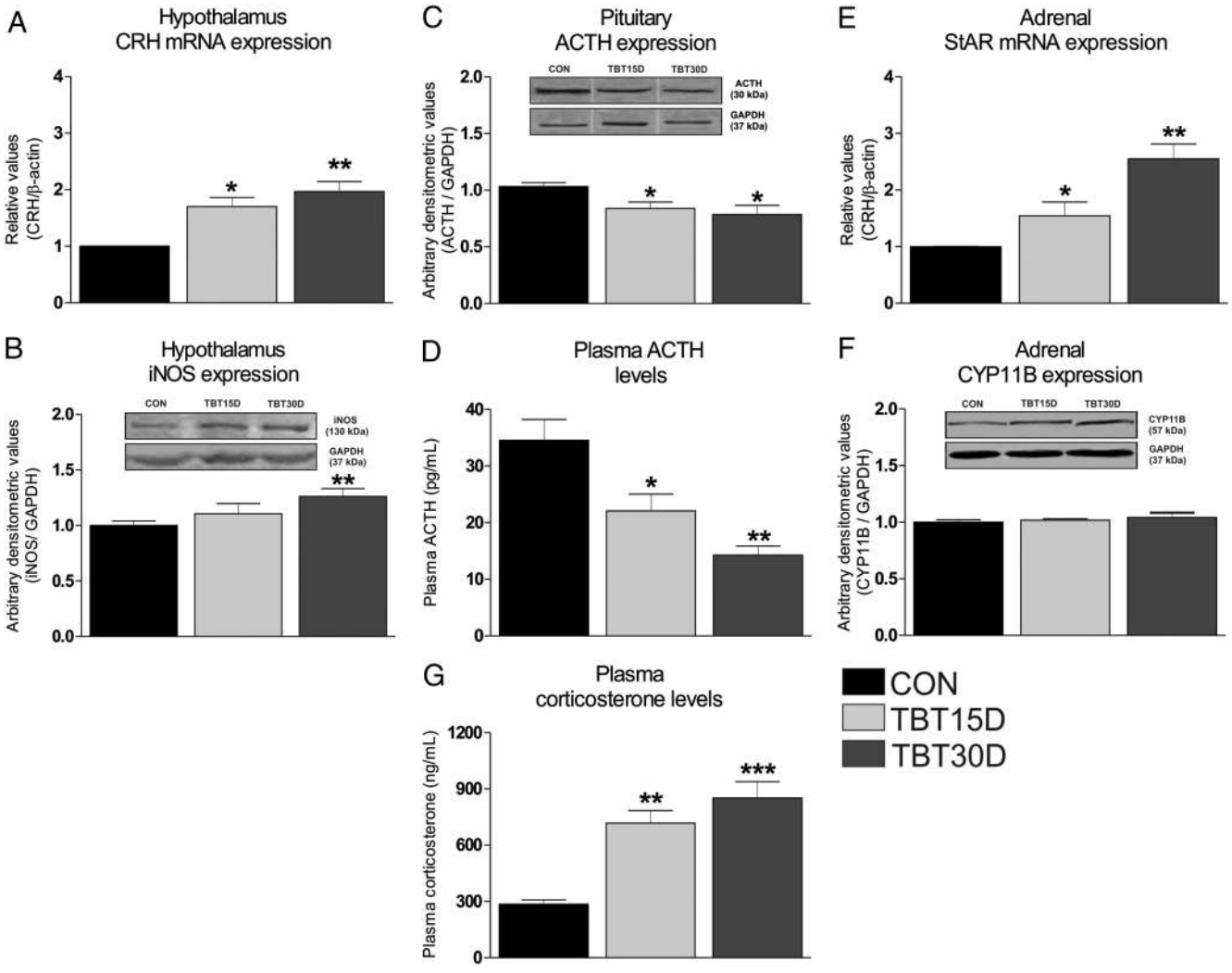

Figure 2. Assessment of hypothalamic CRH and iNOS expression, pituitary ACTH expression, adrenal StAR and CYP_{11B} expression, and plasma ACTH and corticosterone levels. A, qPCR analysis of CRH mRNA extracted from female rat hypothalamic tissue (n = 4). B, An increase in the expression of the iNOS protein in the hypothalamus of TBT30D rats was observed (n = 5). C, Reduced ACTH expression in the pituitaries of TBT15D and TBT30D rats was detected (n = 5). D, Lower plasma ACTH levels were apparent in TBT15D and TBT30D rats (n = 5). E, qPCR analysis of StAR mRNA extracted from female rat adrenal tissues (n = 4). F, Similar CYP_{11B} expression was observed in the adrenals of TBT15D and TBT30D rats (n = 5). G, Increased plasma corticosterone levels were observed in TBT15D and TBT30D rats. One-way ANOVA, Tukey's multiple comparison test; *, $P \leq .05$; **, $P \leq .01$; ***, $P \leq .001$ vs CON.

TBT rats displayed low levels of ACTH expression and basal plasma ACTH

The status of pituitary ACTH expression was determined using Western blot analysis (Figure 2). ACTH expression in the pituitary was lower in both TBT15D and TBT30D rats than in CON rats (CON: 1.03 ± 0.03; TBT15D: 0.84 ± 0.06; TBT30D: 0.79 ± 0.08, n = 5; $P \leq .05$) (Figure 2C). No significant difference in pituitary ACTH expression was observed between TBT15D and TBT30D rats ($P \geq .05$). An ELISA was performed, and plasma ACTH levels were evaluated. A reduction in the basal plasma ACTH levels was observed in both the TBT15D and the TBT30D rats compared with the levels in CON rats (CON: 34.54 ± 3.69; TBT15D: 22.10 ± 2.96; TBT30D: 14.28 ± 1.59 pg/mL, n = 5; $P \leq .01$) (Figure 2D). No significant difference in plasma ACTH levels was observed between TBT15D and TBT30D rats ($P \geq .05$).

Adrenal StAR mRNA expression in TBT rats

StAR mRNA was evaluated in adrenal cortex tissue samples from CON and TBT-treated rats. StAR mRNA in adrenal tissue was higher in both groups of animals exposed to TBT than in CON rats (n = 4, $P \leq .05$) (Figure 2E). No significant differences in adrenal StAR mRNA were detected between TBT15D and TBT30D rats ($P \leq .05$).

Similar CYP_{11B} protein expression and increased basal plasma corticosterone levels in TBT rats

Western blot analysis was performed, and CYP_{11B} protein expression was evaluated in the adrenals (Figure 2). No significantly difference in CYP_{11B} protein expression was observed in the adrenals between TBT rats and CON rats or between the 2 groups of TBT rats (CON: 1.00 ± 0.02; TBT15D: 1.01 ± 0.01; TBT30D: 1.04 ± 0.04, n = 5; $P \geq .05$) (Figure 2F). A RIA was also performed, and plasma corticosterone levels were evaluated. An increase in basal plasma corticosterone levels was observed in both groups of TBT rats compared with the levels in the CON rats (CON: 285.08 ± 23.36; TBT15D: 717.67 ± 66.47; TBT30D: 851.68 ± 87.14 ng/mL, n = 5; $P \leq .001$) (Figure 2G). No significant difference in plasma corticosterone levels was observed between TBT15D and TBT30D rats ($P \geq .05$).

Abnormalities in adrenal morphology in TBT rats

To characterize the effects of TBT on the adrenals, their histology was evaluated using H&E staining (Figure 3). CON adrenals displayed normal characteristics in the adrenal cortex, their adrenal zones and medulla (Figure 3A). The adrenal cortex in both groups of TBT rats exhibited morphological abnormalities, such as adrenal cortex hyperplasia and mitotic activity (arrow Figure 3, B1, C1). The cortical area was increased by approximately 15% in both the TBT15D and TBT30D rats compared with CON rats (CON: 4.06 ± 0.08; TBT15D: 4.67 ± 0.11; TBT30D: 4.71 ± 0.38 mm^2, n = 5; $P \leq .05$) (Figure 3D), but no significant difference was observed in the area of the adrenal cortex between TBT30D and TBT15D rats ($P \geq .05$). No significant differences were observed in the adrenal medulla area or adrenal weight between the CON rats and either group of TBT rats ($P \geq .05$) (data not shown).

Inflammation was increased in the adrenals of TBT rats

Inflammatory cells surrounded the cords of cells in the zona fasciculate and reticularis (asterisk) (Figure 3, B, B1, C, and C1). Adrenal NAG activity was higher in TBT30D rats compared with the levels in CON rats (CON: 0.57 ± 0.02; TBT15D: 0.63 ± 0.06; TBT30D: 0.81 ± 0.07 nmol/μg, n = 5; $P \leq .05$) (Figure 3E). Adrenal NAG activity was similar between CON and TBT15D rats ($P \geq .05$). An increase in adrenal MOP activity was observed in TBT_{30d} rats compared with CON rats (CON: 1.06 ± 0.09; TBT15D: 2.56 ± 0.74; TBT30D: 3.40 ± 0.48 OD/μg, n = 5; $P \leq .01$) (Figure 3I). Adrenal MOP activity was similar between the CON and TBT15D rats ($P \geq .05$). No significant difference in NAG and MOP activity was observed in the adrenals between TBT15D and TBT30D rats ($P \geq .05$). In addition, intense lipid droplet accumulation was observed in both groups of TBT rats (Figure 3, B, B1, C, and C1, arrowhead). Mast cells were identified in the adrenal cortex in CON, TBT15D, and TBT30D rats (Figure 3, F–H). However, a large number of mast cells were observed in the adrenals of both groups of TBT rats (Figure 4, G1 and H1, arrow). The number of mast cells was higher in both groups of TBT rats than the number observed in the CON rats (CON: 0.39 ± 0.01; TBT15D: 0.49 ± 0.02; TBT30D: 0.52 ± 0.02 mast cells/mm^2, n = 5; $P \leq .05$) (Figure 4J). No significant difference in the number of mast cells was observed between TBT15D and TBT30D rats ($P \geq .05$).

Collagen deposition was higher in adrenals of TBT rats

In the adrenal cortex of TBT15D ($P \leq .05$) and TBT30D rats ($P \leq .001$), there was a higher density of superficial collagen than observed in the CON rats (CON: 4.60 ± 0.52; TBT15D: 6.65 ± 0.46; TBT30D: 12.87 ± 1.11%, n = 5; $P \leq .05$) (Figure 3, K–N). In addition, the density was also higher in the TBT30D rats than in the TBT15D rats ($P \leq .001$).

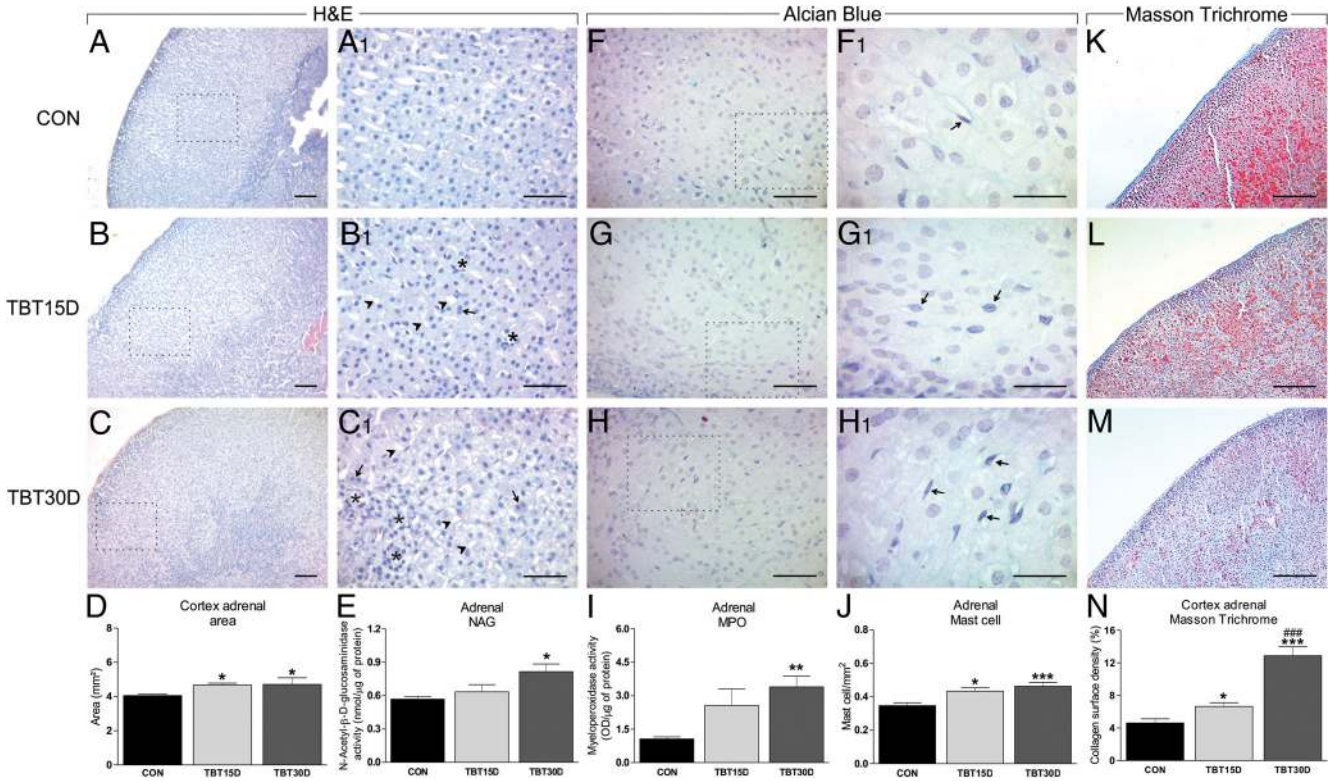

Figure 3. Histomorphology of the adrenals in CON, TBT15D, and TBT30D rats. Representative H&E-stained sections of adrenals obtained from (A and A1) CON, (B and B1) TBT15D, and (C and C1) TBT30D rats (n = 5). Mitosis, arrow; inflammatory cell, asterisk; lipid droplet, arrowhead. D, An increase in the area of the adrenal cortex was observed in both groups of TBT rats (n = 5). E, An increase in NAG activity was observed in the pituitary in TBT30D rats (n = 5). Representative mast cell sections from (F and F1) CON, (G and G1) TBT15D, and (H and H1) TBT30D pituitaries stained with Alcian Blue (arrow) (n = 5). I, Increased MPO activity was observed in the pituitaries of TBT30D rats (n = 5). J, Increased mast cells were observed in the pituitaries of TBT15D and TBT30D rats (n = 5). Representative collagen-stained sections in (K) CON, (L) TBT15D, and (M) TBT30D pituitaries stained with Masson's TM (n = 5). N, Increased collagen surface density was observed in the pituitaries of TBT15D and TBT30D rats (n = 5). Scale bar, 50 μm. One-way ANOVA, Tukey's multiple comparison test; *, $P \leq .05$; **, $P \leq .01$; ***, $P \leq .001$ vs CON; ###, $P \leq .001$ vs TBT15D.

Increased serum cholesterol levels in TBT rats

Cholesterol assays were performed, and serum cholesterol levels were evaluated. Serum cholesterol levels were higher in TBT30D rats than in CON rats (CON: 48.00 ± 1.00; TBT15D: 46.30 ± 4.90; TBT30D: 69.30 ± 6.30 mg/dL, n = 8; $P \leq .05$), and serum cholesterol levels were higher in TBT30D rats than in TBT15D rats ($P < .05$).

Lipid deposition, cholesterol levels, and PPARγ expression were increased in the adrenals of TBT rats

Lipids droplet accumulation in adrenal cortex was analyzed using Oil Red O staining and TEM (Figure 4). An increase in lipid droplet accumulation was observed in the adrenals of TBT rats compared with the adrenals of CON rats (CON: 4.95 ± 0.22; TBT15D: 6.88 ± 0.39; TBT30D: 6.73 ± 0.36%, n = 5; $P \leq .001$) (Figure 4, A, C, E, and G). Similarly, TEM evaluation revealed an increase in adrenal lipid droplet accumulation in both groups of TBT-treated rats (n = 4) (Figure 4, B, D, and F). No significant difference in adrenal lipid droplet accumulation was observed between TBT15D and TBT30D rats ($P \geq .05$). In addition, the adrenal cholesterol levels were higher in in TBT30D rats than in CON rats (CON: 35.58 ± 2.27; TBT15D: 57.29 ± 7.52; TBT30D: 69.76 ± 69.63 mg/dL, n = 8; $P \leq .05$) (Figure 4H). PPARγ is a master regulator of adipocyte differentiation, and TBT has been shown to induce metabolic disruption by modulating PPARγ activity (29, 31). PPARγ expression in the adrenals was determined using Western blot analysis. Adrenal PPARγ expression was higher in both the TBT15D as TBT30D rats than in the CON rats (CON: 1.00 ± 0.03; TBT15D: 1.25 ± 0.02; TBT30D: 1.36 ± 0.59, n = 5; $P \leq .01$) (Figure 4I). Adrenal PPARγ expression was similar between TBT15D and TBT30D rats ($P \geq .05$).

O_2^- levels in the pituitary and adrenals and apoptotic markers were more highly expressed in TBT rats

To analyze the production of O_2^- in the pituitary and adrenals, DHE marking was performed (Figure 5). In the

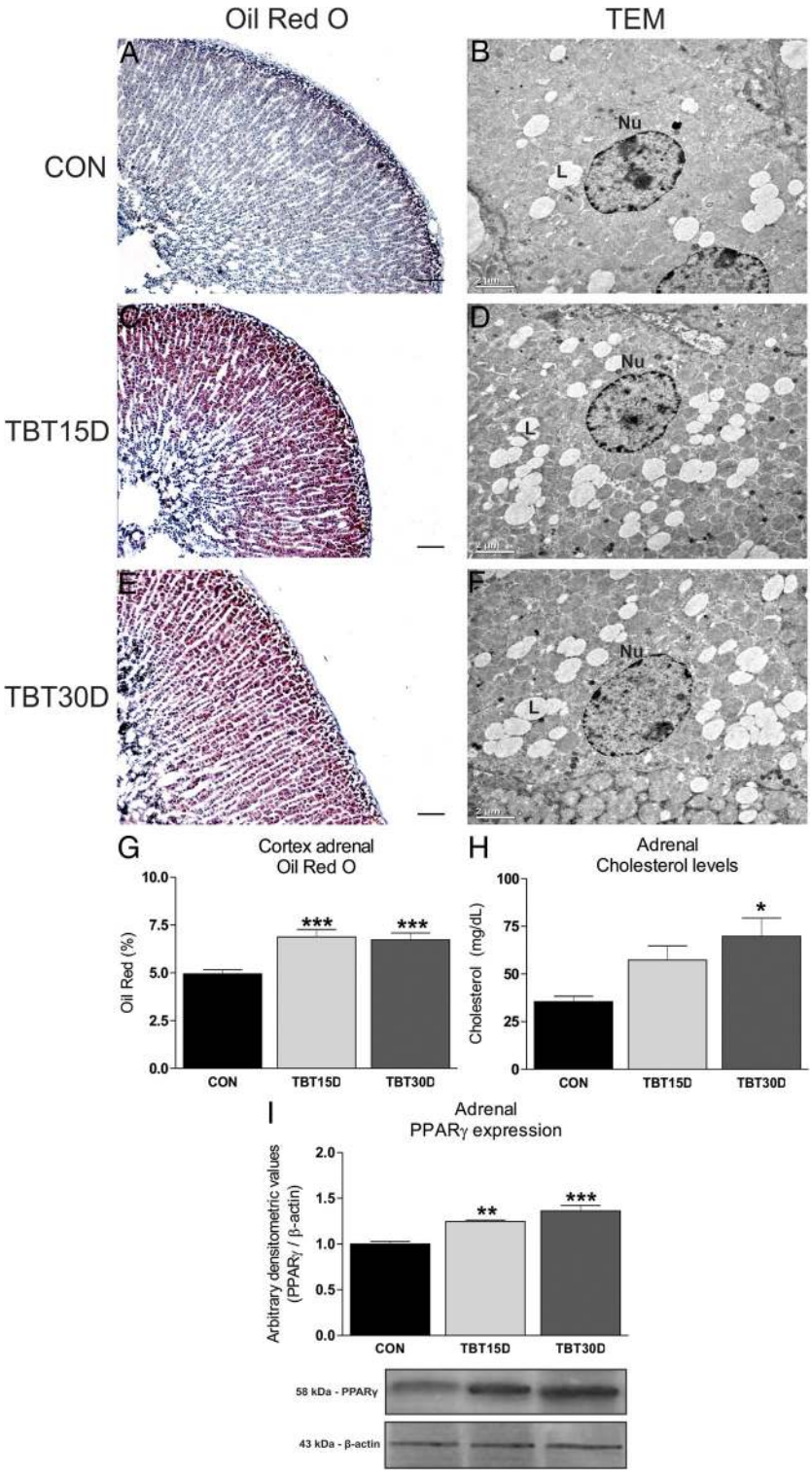

Figure 4. Assessment of lipid droplet accumulation and Western blot analysis for the PPARγ protein in the adrenals of CON, TBT15D, and TBT30D rats. Representative lipid droplet-stained sections of adrenals were obtained from (A) CON, (C) TBT15D, and (E) TBT30D rats using Oil Red O (n = 5). G, Higher lipid droplet accumulation was observed in the adrenals of TBT15D and TBT30D rats (n = 5). B, TEM demonstrating the normal zona fasciculada (ZF) of the adrenal cortex in CON rats. D and F, Abnormal lipid droplet accumulation in the ZF of the adrenal cortex in TBT15D and TBT30D rats (n = 4). H, Elevated cholesterol levels were observed in the adrenals in TBT rats (n = 8). I, Analysis of the expression of the PPARγ protein in the adrenals of TBT15D and TBT30D rats (n = 5). Scale bars, 200 μm (A, C, and E) and 2 μm (B, D, and F). Nu, nucleus; L, lipid droplet. One-way ANOVA, Tukey's multiple comparison test; **, $P \leq .01$; ***, $P \leq .001$ vs CON.

pituitary, we detected an increase in O_2^- levels in both TBT15dand TBT30d rats compared with the CON rats (CON: 8.95 ± 0.56; TBT15D: 15.54 ± 1.14; TBT30D: 12.83 ± 0.63, n = 5; $P \leq .001$) (Figure 5, A, C, E, and G). No significant difference in O_2^- levels was observed in the pituitary between TBT15D and TBT30D rats ($P \geq .05$). In addition, the expression of the pituitary caspase-3 protein was determined. Pituitary caspase-3 expression was higher in both groups of TBT rats than in the CON rats (CON: 1.00 ± 0.04; TBT15D: 1.22 ± 0.04; TBT30D: 1.35 ± 0.09, n = 5; $P \leq .05$) (Figure 5I). The adrenal cortex O_2^- production was higher in both groups of TBT rats than in the CON rats (CON: 0.09 ± 0.01; TBT15D: 0.23 ± 0.01; TBT30D: 0.38 ± 0.01, n = 5; $P \leq .001$) (Figure 5, B, D, F, and H). A raise in adrenal O_2^- production was also observed in TBT30d rats compared with TBT15d rats ($P \leq .05$). In addition, adrenal caspase-3 expression was higher in both groups of TBT rats than in the CON rats (CON: 1.02 ± 0.02; TBT15D: 1.34 ± 0.11; TBT30D: 1.51 ± 0.23, n = 5; $P \leq .05$) (Figure 5J). Caspase-3 expression in the pituitary and adrenals was similar between TBT15D and TBT30D rats ($P \geq .05$).

Restraint stress assessment in TBT rats

The 30-minute restraint stress was associated with a significant increase in the plasma levels of ACTH in all groups, which returned to baseline 30 minutes after the termination of stress (Figure 6). Restraint stress evoked a significantly higher response in both groups of TBT rats compared with the CON rats, which was evident 30 minutes after initiation of restraint stress (CON: 66.16 ± 11.41; TBT15D: 141.33 ± 25.66; TBT30D: 116.50 ± 10.50,

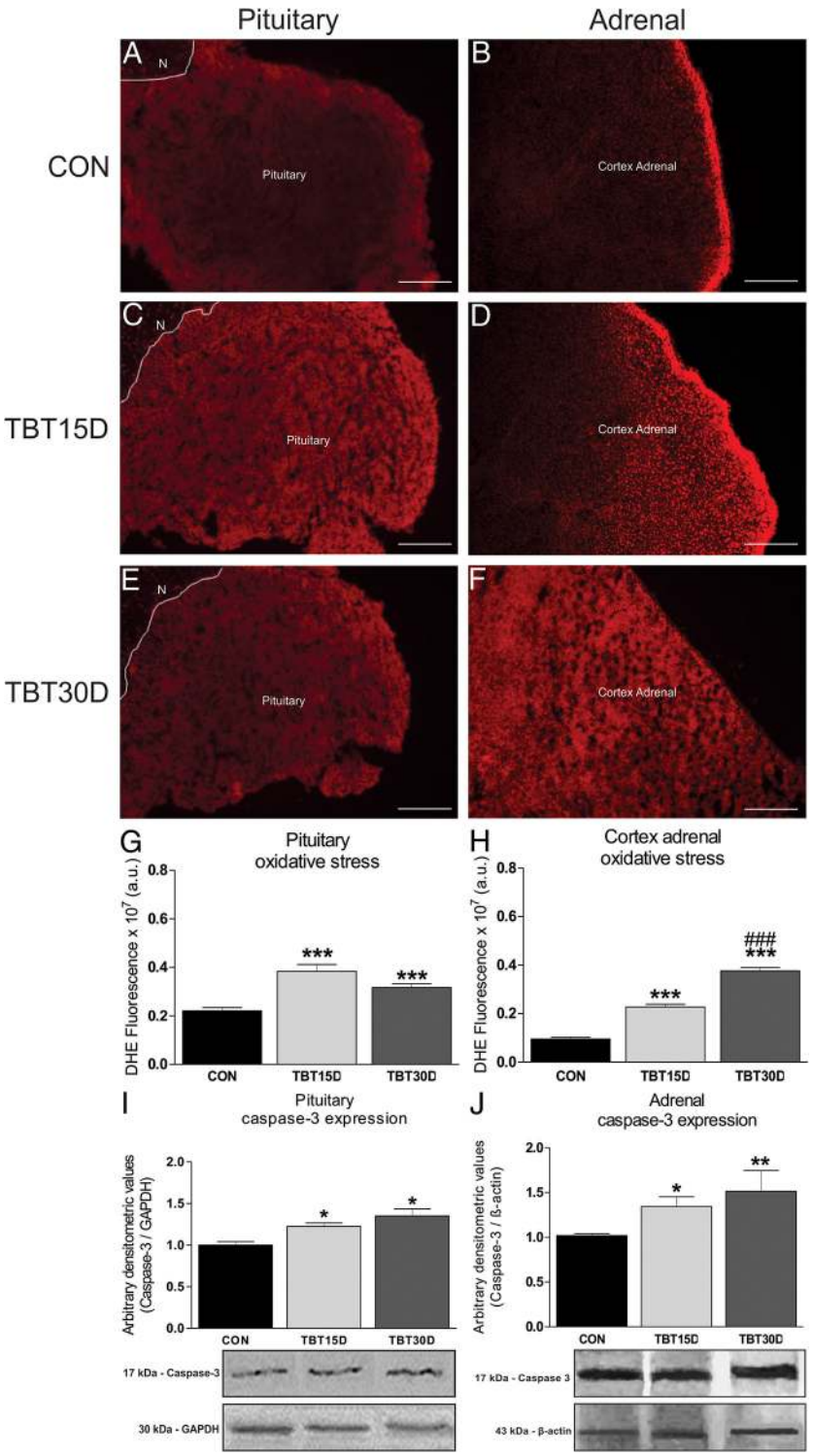

Figure 5. In situ detection of superoxide anion (O_2^-) production and Western blot analysis of caspase-3 protein expression in the pituitaries and adrenals of CON, TBT15D, and TBT30D rats. Fluorescence micrographs stained with the O_2^--sensitive dye DHE (red fluorescence) were obtained from (A) CON, (C) TBT15D, and (E) TBT30Dpituitaries and from (B) CON, (D) TBT15d, and (F) TBT30D adrenal glands (n = 5). G, Increased production of O_2^- level was observed in the pituitaries of TBT15D and TBT30D rats (n = 5). H, Increased production of O_2^- level was observed in the adrenal cortex in TBT15D and TBT30D rats (n = 5). I, Analysis of Casp-3 protein expression levels in the pituitary gland in TBT15D and TBT30D rats (n = 5). J, Analysis of Casp-3 protein expression levels in adrenals in TBT15D and TBT30D rats (n = 5). Pituitary, anterior pituitary; N, neurohypophysis; Casp-3, caspase-3. Scale bar, 400 μm. One-way ANOVA, Dunn's multiple comparison test; *, $P \leq .05$; **, $P \leq .01$; ***, $P \leq .001$ vs CON; ###, $P \leq .001$ vs TBT15D.

n = 5; $P \leq .01$) (Figure 6A). Hypothalamic CRH mRNA was evaluated in the CON rats and both groups of TBT rats submitted to 30 minutes of restraint stress. CRH mRNA was approximately 40%–70% higher in samples of hypothalamic tissue from both groups of TBT-treated rats compared with CON rats (n = 4, $P \leq .05$) (Figure 6B). No significant differences in hypothalamic CRH mRNA were observed in TBT15D and TBT30D rats ($P \geq .05$).

Glucocorticoid negative feedback in TBT rats

The plasma ACTH levels in ADX CON rats were significantly higher than those in intact CON rats (ADX CON: 106.67 ± 8.81 ng/mL, n = 4 vs intact CON: 34.54 ± 3.69 pg/mL, n = 5; $P \leq .001$) (Figure 6C). The plasma ACTH levels in both groups of ADX TBT rats were significantly higher than those in both intact TBT rats (ADX TBT15D: 160.50 ± 4.91 ng/mL, n = 4 vs intact TBT15D: 22.10 ± 2.96; ADX TBT30D: 69.40 ± 7.70 pg/mL, n = 4 vs intact TBT30D: 14.28 ± 1.59 ng/mL, n = 5; $P \leq .001$) (Figure 6C). Interestingly, the plasma ACTH levels in the ADX TBT15D group were approximately 50% higher than the ACTH levels in ADX CON rats ($P < .001$). The plasma ACTH levels were reduced by approximately 30% in ADX TBT30D rats compared with ADX CON rats ($P < .001$). Additionally, the plasma ACTH levels were approximately 50% lower in ADX TBT30D rats than they were in ADX TBT15D rats ($P < .001$), possibly due to the impairment of negative feedback by glucocorticoids in TBT treated female rats. Hypothalamic CRH mRNA was evaluated in intact and ADX CON and both groups of TBT rats. Hypothalamic CRH mRNA expression in ADX CON rats was significantly higher than CRH

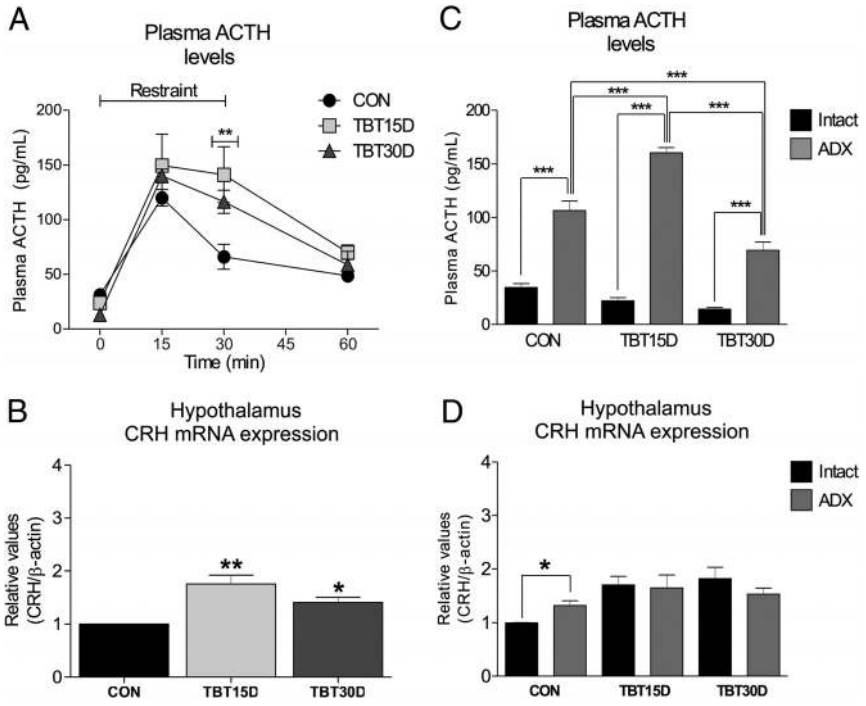

Figure 6. Restraint stress and assessment of glucocorticoid negative feedback in CON, TBT15D, and TBT30D rats. A, Plasma ACTH levels in CON, TBT15D, and $TBT30D_{30d}$ rats before (0 min [n = 5], 15 min [n = 5], and 30 min [n = 5]) and after 30 minutes of restraint stress (n = 5). B, qPCR analysis of CRH mRNA extracted from hypothalamic tissue in female rats submitted to 30 minutes of restraint stress (n = 4). C, Plasma ACTH levels in intact CON, TBT15D, and TBT30D rats compared with ADX CON, ADX TBT15D, and ADX TBT30D rats, respectively (n = 4). D, Hypothalamic CRH mRNA from intact CON, TBT15D, and TBT30D rats compared with ADX CON, ADX TBT15D, and ADX TBT30D rats, respectively (n = 4). One- and two-way ANOVA, Tukey's multiple comparison test, n = 4–5; **, $P \leq .01$; ***, $P \leq .001$ vs CON.

mRNA expression in intact CON rats ($P \leq .05$) (Figure 6D). However, both ADX TBT15D and TBT30D rats exhibited a similar increase in CRH mRNA levels when compared with the respective intact groups ($P \geq .05$, n = 4). CRH mRNA levels were not significantly different among ADX CON, TBT15D, and TBT30D rats ($P \geq .05$).

Discussion

In this study, we provide evidence showing that TBT disrupts the morphophysiology of the HPA axis in female rats, leading to an increased in CRH mRNA expression, decreased in ACTH release and increased in corticosterone levels. This hormonal dissociation could be associated with inflammation and iNOS expression in the hypothalamus. In addition, an increase in inflammation, OSs, apoptosis, and collagen deposition in the pituitary and adrenal glands were observed in TBT rats.

Previous studies have reported that OTs play a direct role in the improper functioning of the HPA axis (Table 1) (36, 37, 54–57). Wester et al (36) reported that exposure to bis (trin-butyltin) oxide (TBTO) at 50 mg/kg for 106 weeks increased pituitary weight in female rats. Our results agree with these previous findings. We observed a small increase in the size of the pituitary and an increase in pituitary weight in the TBT30d rats. Krajnc et al (55) surprisingly found no change in rat pituitary weight after exposure to 80 mg/kg of TBTO for 28 days, which is in contrast to the results in our model. This exposure may not result in stimulation of the pituitary-adrenal axis (55). Inflammation affects various steps of pituitary hormonal regulation (58, 59). In our study, the TBT rats displayed distinct evidence of pituitary inflammation. A common feature of mammalian hypophysitis is the presence of different inflammatory cells, such as macrophages (60, 61). In our study, the TBT30D pituitary exhibited higher NAG and MPO activity, suggesting a role for macrophages and neutrophils in the inflammatory process. Mast cells are also part of immune responses, and they are involved in nonspecific inflammatory disorders and tissue remodeling (62, 63). In our study, the pituitaries of both groups of TBT rats showed an increase in mast cell numbers. Vidal et al (60) described a significant role for mast cells in human adenohypophysitis. Furthermore, studies related that abnormal collagen deposition was triggered in pituitary histopathologies, such as adenohypophysitis (64, 65). Similarly, Rotondo et al (61) reported the accumulation of collagen in a rat adenohypophysitis model. Our results agree with these previous findings in that they show an increase in collagen deposition in the pituitary in both groups of TBT rats. Thus, an increase in inflammation and collagen deposition in the pituitary of TBT rats could be associated with the dysfunction.

From previous studies, we learned that CRH and ACTH play critical roles in the proper function of the HPA axis (66, 67). Studies have shown that xenobiotics could be modulating the HPA axis (56, 68). Chen et al (69) reported an increase in CRH expression and ACTH levels in the male offspring of pregnant rats that had been exposed to bisphenol A (2 μg/kg) from gestation day 10 to lactation day 7. In contrast, Pereiro et al (44) reported a down-regulation of HPA axis components in rats treated with 0.5, 1.0, 3.0, and 6.0 mg of perfluorooctane sulfonate

Table 1. Summary of Changes to the HPA Axis Induced by OTs

	Animal-Model/OTs/Dose						
HPA Axis Parameter	**Rat/TBTO (100–1560 mg/kg)**	**Rat/TBTO (20–80 mg/kg)**	**Rat/TBTO (50 mg/kg)**	**Bovine Adrenal Cells/TBT (3.52–3520 × 10^{-4} mg/L)**	**Mice/TMT (3 mg/kg)**	**Zebrafish/TBT (105.6–1760 × 10^{-4} mg/L)**	**Rat/TBT (10^{-4} mg/kg)**
Time of exposure	Chronic	Chronic	Chronic	Acute	Acute	Acute	Sub/chronic
Pituitary							
Organ weight	NR	↔	↑	NA	NR	NR	↑
Morphology	Impaired	NR	NR	NA	NR	NR	Impaired
Inflammation process	NR	NR	NR	NA	NR	NR	↑
Collagen deposition	NR	NR	NR	NA	NR	NR	↑
OS development	NR	NR	NR	NA	NR	NR	↑
Apoptosis marker	NR	NR	NR	NA	NR	NR	↑
ACTH expression	↓	↔	NR	NA	NR	NR	↓
Adrenal							
Morphology	Impaired	↔	Impaired	NR	NR	NR	Impaired
Inflammation process	NR	NR	NR	NA	NR	NR	↑
Collagen deposition	NR	NR	NR	NR	NR	NR	↑
OS development	NR	NR	NR	NR	NR	NR	↑
Apoptosis marker	NR	NR	NR	NR	NR	NR	↑
Lipids droplets accumulation/ PPARγ expression	↑/NR	NR	NR	NR	NR	NR	↑/↑
Glucocorticoids signaling	NR	NR	NR	↔/↓	NR	↔/↓	Impaired
HPA axis							
ACTH levels	NR	NR	NR	NA	NR	NR	↓
Corticosteroids levels	↑	↔	NR	↔/↓	↑	NR	↑
Corticosteroid CON feed back	NR	NR	NR	NA	NR	NR	NR
HPA function	↓	↔	NR	NA	NR	NR	↓
Reference	Funahashi et al 54	Krajnc et al 55	Wester et al 36	Yamazaki et al 36	Morita et al 56	Weger et al 57	This study

Summary of HPA axis changes induced by OTs. TMT, trimethyltin; ↑, increased; ↓, decreased; ↔, unchanged or similar to CON; NR, not reported; NA, not applicable.

per kg/d for 28 days. Funahashi et al (54) reported that TBTO reduced the amount of ACTH-immunohistochemical-positive staining in corticotrophs and increased serum corticosterone levels in rats. In addition, the HPA axis activity could be influenced by inflammatory signals (63, 70). In many patients with severe inflammation, low plasma ACTH levels and normal or elevated cortisol levels are observed in the early period following admission to an intensive care station (71). It has been proposed that increased levels of proinflammatory mediators, such as TNFα and IL-1β, can directly impair the CRH-stimulated release of ACTH (72). Interferon-γ caused the dose-dependent inhibition of corticotropin-releasing factor-stimulated ACTH secretion in rat pituitary cells (73). Polito et al (74) described a reduction in ACTH expression and an increase in CRH and iNOS expression in the hypothalamus of a rat sepsis model. Our study is in agreement with these previous findings, revealing that both groups of TBT-treated rats displayed an increase in hypothalamic CRH and iNOS expression, a reduction in ACTH expression and plasma ACTH levels and an increase in plasma corticosterone levels. Another study reported that nitric oxide stimulated CRH expression and suppressed the stimulatory effects of vasopressin on ACTH secretion in a rat sepsis model (75). The CRH neurons are found mainly in the hypothalamic PVN nucleus (4–5). However, CRH expression is present in other brain regions including limbic, the nucleus of the stria terminalis, the central nucleus of the amygdala, etc (76). CRH at these sites plays an important role in response to stress, as shown in the central amygdaloid nucleus in rat submitted to stress (77, 78). Thus, an increase in inflammation and iNOS protein expression in TBT rats could be associated with the impairment of CRH-stimulated ACTH release, leading to hormonal dissociation. Other factors, as a repeated exposure to the same stressor could be associated with hormonal dissociation, and it is possible the CRH mRNA does not reflect portal vein CRH levels (Figure 7) (71, 79). However, other studies have suggested that decreased ACTH secretion may be the result of a negative regulatory effect induced by chronically elevated glucocorticoid levels, as has been observed in patients with systemic inflammation (80–82) and our data. Thus, the adrenal inflammation could be associated with an increase in corticosterone levels and a reduction in ACTH levels in TBT rats.

A restraint stress test was performed to evaluate hypothalamic and pituitary function in CON rats and both groups of TBT-treated rats. Similar to the findings of Stinnett et al (83) and Felszeghy et al (52), we observed that restraint stress was associated with an increase in CRH expression and plasma ACTH levels in all rats analyzed. However, both groups of TBT rats exhibited elevated CRH expression and increased ACTH levels in response to stress within 30 minutes, thus demonstrating that HPA

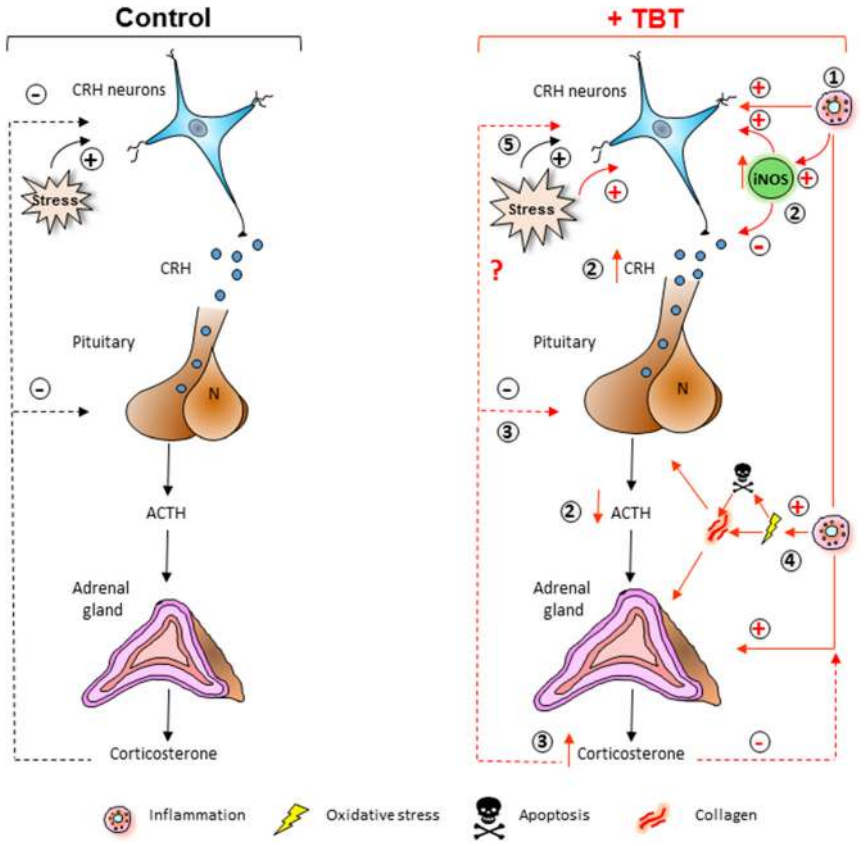

Figure 7. A model of the potential mechanism of modulation of the HPA axis by TBT. TBT leads to morphophysiological abnormalities (red line) such as: 1) TBT leads to inflammation that stimulates hypothalamic CRH mRNA and iNOS protein expression. 2) The hypothalamic iNOS protein expression could be associated with the impairment of CRH-stimulated ACTH release. 3) A decreased ACTH secretion may also be the result of a negative regulatory effect induced by elevated corticosterone levels. 4) TBT leads to inflammation that stimulates pituitary and adrenal OS, apoptosis, and collagen deposition. 5) And TBT increased the stress and CRH mRNA expression in the hypothalamus of female rats.

activity was abnormal. In addition, Dhabhar et al (84) suggested that a repeated and chronic exposure to the same stressor can result in habituation of the HPA axis response, characterized by a decreasing the HPA axis response over time, as shown apparently in TBT30D rats.

To determine the role of glucocorticoid negative feedback on HPA axis activity in TBT rats, ADX was performed in animals from both groups. Both groups of TBT rats responded with an exaggerated increase in plasma ACTH levels and no change in CRH expression. These results were apparent in both groups of TBT-treated ADX rats. The effects of EDCs on TBT may involve complex alterations of different components of the rat HPA axis, as previously demonstrated by Xia et al (43) using the perfluorooctane sulfonate exposure. In addition, the abnormal HPA axis function in TBT-treated ADX rats may involve other factors could be associated a hormonal dissociation, as metabolic disease and inflammation (71, 85), as result of TBT exposure (29, 31). Similarly, the habituation of the HPA axis could be associated a decreasing the HPA axis response in the TBT30D rats. These data suggest an abnormal central glucocorticoid negative feedback on ACTH secretion.

In addition, TBT impaired steroidogenesis in both in vivo and in vitro models (28, 38, 86). Yamazaki et al (37) reported a reduction in $P450_{c21}$ and $P450_{11\beta}$ mRNA expression levels in adrenal bovine cells that were treated with TBT for 48 hours (10nM and 100nM). However, the same study reported no significant difference in adrenal StAR, $P450_{scc}$ and $P450_{3\beta\text{-HSD}}$ mRNA expression levels. Mitra et al (87) described an increase in StAR expression in rat Leydig cells exposed to TBT 600nM for 1 hour. Our results demonstrated an increase in adrenal StAR expression in both groups of TBT-treated rats and no significant difference in adrenal CYP_{11B} expression in all groups. In previous studies, we reported that the major regulatory step of steroidogenesis is cholesterol transport to the mitochondrial inner membrane, which is stimulated by the StAR (88). However, the control of StAR expression is complex and involves several steps, both transcriptionally and posttranscriptionally (89). Thus, the effects of steroidogenesis in the adrenal cortex of TBT rats could involve abnormal StAR expression.

The adrenals are a common target organ between stress and xenobiotic exposure models (14, 15, 90). Milovanović et al (91) reported that a single instance of exposure to ethanol at 4 g/kg raised the diameter of adrenal cortex in female rats. Similarly, in our study, both TBT_{15d} and TBT_{30d} rats displayed an increase in the area of the adrenal cortex. Thus, exposure to TBT leads to adrenal cortex hypertrophy and could be associated with adrenal dysfunction. Several immuno-endocrine interactions have been described in adrenal immune cells such as macrophage and mast cell activation (92–94). During systemic inflammation, immune cells play relevant role in adrenal function (95, 96). Kanczkowski et al (80), using an lipopolysaccharide mouse model, demonstrated that the rapid infiltration of neutrophils into the adrenals was induced by increased MPO activity. In our study, the TBT_{30d}

adrenals showed higher NAG and MPO activity, suggesting a role for macrophages and neutrophils in adrenal inflammation. In addition, Kim et al (97) described a role for mast cells in adrenal hyperplasia in numerous mouse strains, including BALB/c and C57BL/6 mice. In our study, the adrenals of both groups of TBT rats showed a higher number of mast cells, suggesting that mast cells also play a role in adrenal inflammation. Among other abnormalities, TBT has been reported to induce cellular damage that can be replaced by fibrous tissue (38, 39, 41). In agreement with these previous findings, both groups of TBT rats displayed an increase in collagen deposition in the adrenal cortex in a time-dependent manner. Reed et al (98) reported that adrenal fibrosis was associated with adrenal inflammation in a 55-year-old man. Thus, the adrenal abnormalities observed in both groups of TBT rats could be associated with the direct toxic effects of TBT.

In a previous study in our laboratory (31), TBT15D rats exhibited no change in serum cholesterol levels. However, in the TBT30D rats of this study, higher serum and adrenal cholesterol levels were observed. Similar our data, Xia et al (43) observed a reduction in serum ACTH levels and an increase in serum cholesterol levels in the offspring of pregnant rats that were exposed to 4-g ethanol per kg/d for 10 days. A constant supply of cholesterol is known to be required in adrenal steroidogenesis modulated by StAR function (88, 99, 100). Lipid accumulation in cholesterol-laden lipoid structures in the adrenal cortex zones also occurs during other abnormal states associated with decreased cholesterol utilization, such as chronic treatment with the inhibitor of $P450_{scc}$ or abnormal StAR function (101–104). Our data demonstrated an abnormal pattern of StAR expression in the adrenal cortex of TBT rats.

In addition, TBT exposure results in various degrees of adiposity and induces metabolic disorders by modulating PPARγ activity (29, 105–110). In agreement with these previous findings, both groups of TBT rats displayed distinct evidence of an increase in lipid droplet accumulation and PPARγ protein expression levels in the adrenal cortex. In a previous study, we reported an increase in lipid droplet accumulation and PPARγ protein expression in the liver in TBT15D rats (31). The accumulation of adrenal lipid droplets is associated with an early steroidogenic pathway blockade and/or abnormal StAR functioning (83, 104). However, it is possible that TBT affects adrenocortical function, leading to abnormal StAR or other steroidogenic enzyme function. The ACTH-independent production of corticosterone or TBT may involve PPARγ signaling pathways and other nuclear receptors, as shown in other EDC effects of TBT (31, 107). The dramatic nature of these findings is therefore not fully understood.

Several studies have reported that imbalances in OS levels lead to the dysfunctions (111–113). TBT up-regulates the cell redox balance in brain areas, such as the hypothalamus, resulting in an increase in the reactive oxygen species and cellular damage (30, 114). Annabi et al (115) reported that imidacloprid insecticide, applied at 40 mg/kg for 28 days, increased malondialdehyde levels in the

Table 2. Antibody Table

Peptide/Protein Target	Antigen Sequence (if Known)	Name of Antibody	Manufacturer, Catalog Number, and/or Name of Individual Providing the Antibody	Species Raised in; Monoclonal or Polyclonal	Dilution Used	Reference
Caspase-3	1–277 of the procaspase-3 of human	Caspase-3 antibody (H-277)	Santa Cruz Biotechnology, Inc, sc-7148	Rabbit	1:500	124
Anti-ACTH	(1–24)	ACTH	Chemicon International, AB-902	Rabbit; polyclonal	1:800	125
β-Actin		β-Actin antibody (R-22)	Santa Cruz Biotechnology, Inc, sc-130657	Rabbit; polyclonal	1:1000	31
PPARg	Specific for an epitope mapping between amino acids 480 and 505 at the C terminus of PPARγ of human origin	PPARγ antibody (E-8)	Santa Cruz Biotechnology, Inc, sc-7273	Mouse; monoclonal	1:500	126
$CYP_{11B}1/2$	204–503 (deletion 401–466)	$CYP_{11B}1/2$ (H-300)	Santa Cruz Biotechnology, Inc, sc-28205	Rabbit; polyclonal	1:500	127
iNOS	Mouse iNOS aa. 961–1144	Purified mouse antimouse iNOS/NOS type II	BD Transduction Laboratories-610328	Mouse; monoclonal	1:1500	128
GAPDH	1–335	GAPDH (FL-335)	Santa Cruz Biotechnology, Inc, sc-25778	Rabbit; polyclonal	1:1000	129
Rabbit immunoglobulin IgG	Purified rabbit IgG as the immunogen	Goat antirabbit IgG-alkaline phosphatase conjugate	Sigma-Aldrich, A-3687	Rabbit; polyclonal	1:1000	31
Mouse immunoglobulin IgG	Purified mouse IgG	Goat antimouse IgG-alkaline phosphatase conjugate	Sigma-Aldrich, A-3562	Mouse; polyclonal	1:1000	31

rat hypothalamus and pituitary. Our results agree with these previous findings by showing higher OS levels in the pituitary and adrenals in both groups of TBT rats. Kaida et al (116) and Brown et al (117) reported that activation of mast cells and neutrophils leads to OS in rat adrenal tissue and other tissues. Our results demonstrate that mast cells and neutrophils are active in both the pituitary and the adrenal gland. Several studies have reported that elevated reactive oxygen species activity has been associated with apoptosis and caspase pathway activation, which can lead to alterations in cellular functioning (118–120). Several studies have reported that TBT induced apoptosis in different cell models, such as rat thymocytes, human T cells, and Jurkat cells (27, 121–123). Our results agree with these previous findings by showing higher caspase-3 protein expression in the pituitary and adrenals in both groups of TBT rats.

In conclusion, our female rat model demonstrates that abnormal HPA axis function is attributable to the disruptive effects of TBT on the HPA axis. TBT induced a dissociation between CRH, ACTH, and corticosterone hormones, that could be associated an inflammation and increased of iNOS expression in hypothalamus. Furthermore, the inflammation, OS, apoptosis, and fibrosis were observed in pituitary and adrenal glands of TBT rats. This work increases our understanding of the toxic effects of TBT at different levels on the HPA axis.

Acknowledgments

Address all correspondence and requests for reprints to: Professor Dr Jones B. Graceli, Laboratório de Endocrinologia e Toxicologia Celular, Departamento de Morfologia/CCS, Universidade Federal do Espírito Santo, Avenida Marechal Campos 1468, Prédio do Básico I, Sala 5, 290440-090 Vitória, ES, Brasil. E-mail: jbgraceli@gmail.com.

This work was supported by Fundação de Amparo à Pesquisa e Inovação do Espírito Santo Grant 0609-2015 and Auxílio Básico à Pesquisa da Fundação de Amparo à Pesquisa do Estado do Rio de Janeiro Grant E-26/110.485/2014.

Disclosure Summary: The authors have nothing to disclose.

References

1. **Spiess J, Rivier J, Rivier C, Vale W.** Primary structure of corticotropin-releasing factor from ovine hypothalamus. *Proc Natl Acad Sci USA*. 1981;78:6517–6521.
2. **de Kloet ER, Joëls M, Holsboer F.** Stress and the brain: from adaptation to disease. *Nat Rev Neurosci*. 2005;6:463–475.
3. **Fowden AL, Li J, Forhead AJ.** Glucocorticoids and the preparation for life after birth: are there long-term consequences of the life insurance? *Proc Nutr Soc*. 1998;57:113–122.
4. **Chen R, Lewis KA, Perrin MH, Vale WW.** Expression cloning of a human corticotropin-releasing-factor receptor. *Proc Natl Acad Sci USA*. 1993;90:8967–8971.
5. **Nicolaides NC, Kyratzi E, Lamprokostopoulou A, Chrousos GP, Charmandari E.** Stress, the stress system and the role of glucocorticoids. *Neuroimmunomodulation*. 2015;22:6–19.
6. **Moisiadis VG, Matthews SG.** Glucocorticoids and fetal programming part 1: outcomes. *Nat Rev Endocrinol*. 2014;10:391–402.
7. **Yoshimura F, Harumiya K, Suzuki N, Totsuka S.** Light and electron microscopic studies on the zonation of the adrenal cortex in albino rats. *Endocrinol Jpn*. 1968;15:20–52.
8. **Whitworth E, Vinson GP.** Zonal differentiation in the rat adrenal cortex. *Endocr Res*. 2000;26:973–978.
9. **Zelander T.** The ultrastructure of the adrenal cortex of the mouse. *Z Zellforsch Mikrosk Anat*. 1957;46:710–716.
10. **Pihlajoki M, Dorner J, Cochran RS, Heikinheimo M, Wilson DB.** Adrenocortical zonation, renewal, and remodeling. *Front Endocrinol (Lausanne)*. 2015;6:27.
11. **Hinson JP, Raven PW.** Effects of endocrine-disrupting chemicals on adrenal function. *Best Pract Res Clin Endocrinol Metab*. 2006;20:111–120.
12. **Gore AC.** Neuroendocrine targets of endocrine disruptors. *Hormones (Athens)*. 2010;9:16–27.
13. **Moisiadis VG, Matthews SG.** Glucocorticoids and fetal programming part 2: mechanisms. *Nat Rev Endocrinol*. 2014;10:403–411.
14. **Rosol TJ, Yarrington JT, Latendresse J, Capen CC.** Adrenal gland: structure, function, and mechanisms of toxicity. *Toxicol Pathol*. 2001;29:41–48.
15. **Harvey PW.** Adrenocortical endocrine disruption. *J Steroid Biochem Mol Biol*. 2016;155(pt B):199–206.
16. **Hinson JP, Raven PW.** DHEA deficiency syndrome: a new term for old age? *J Endocrinol*. 1999;163:1–5.
17. **Boyer IJ.** Toxicity of dibutyltin, tributyltin and other organotin compounds to humans and to experimental animals. *Toxicology*. 1989;55:253–298.
18. **IPCS.** *World Health Organization's International Programme on Chemical Safety, Global Assessment of the State-of-the-Science of Endocrine Disruptors, IPCS*. Geneva, Switzerland: World Health Organization; 2002.
19. **Latini G.** Monitoring phthalate exposure in humans. *Clin Chim Acta*. 2005;361:20–29.
20. **Jenkins S, Raghuraman N, Eltoum I, Carpenter M, Russo J, Lamartiniere CA.** Oral exposure to bisphenol an increases dimethylbenzanthracene-induced mammary cancer in rats. *Environ Health Perspect*. 2009;117:910–915.
21. **Diamanti-Kandarakis E, Bourguignon JP, Giudice LC, et al.** Endocrine-disrupting chemicals: an Endocrine Society scientific statement. *Endocr Rev*. 2009;30:293–342.
22. **Fent K.** Ecotoxicology of organotin compounds. *Crit Rev Toxicol*. 1996;26:1–117.
23. **Graceli JB, Sena GC, Lopes PF, et al.** Organotins: a review of their reproductive toxicity, biochemistry, and environmental fate. *Reprod Toxicol*. 2013;36:40–52.
24. **Whalen MM, Loganathan BG, Kannan K.** Immunotoxicity of environmentally relevant concentrations of butyltins on human natural killer cells in vitro. *Environ Res*. 1999;81:108–116.
25. **HELCOM.** Hazardous substances in the Baltic Sea. An integrated thematic assessment of hazardous substances in the Baltic Sea. *Balt Sea Environ Proc*. 2010;120B.
26. **Wiebkin P, Prough RA, Bridges JW.** The metabolism and toxicity of some organotin compounds in isolated rat hepatocytes. *Toxicol Appl Pharmacol*. 1982;62:409–420.
27. **Stridh H, Cotgreave I, Müller M, Orrenius S, Gigliotti D.** organotin-induced caspase activation and apoptosis in human peripheral blood lymphocytes. *Chem Res Toxicol*. 2001;14:791–798.
28. **Grote K, Stahlschmidt B, Talsness CE, Gericke C, Appel KE, Chahoud I.** Effects of organotin compounds on pubertal male rats. *Toxicology*. 2004;202:145–158.

29. **Grün F, Watanabe H, Zamanian Z, et al.** Endocrine-disrupting organotin compounds are potent inducers of adipogenesis in vertebrates. *Mol Endocrinol*. 2006;20:2141–2155.
30. **Mitra S, Gera R, Siddiqui WA, Khandelwal S.** Tributyltin induces oxidative damage, inflammation and apoptosis viadisturbance in blood–brain barrier and metal homeostasis in cerebral cortex of rat brain: an in vivo and in vitro study. *Toxicology*. 2013;310:39–52.
31. **Bertuloso BD, Podratz PL, Merlo E, et al.** Tributyltin chloride leads to adiposity and impairs metabolic functions in the rat liver and pancreas. *Toxicol Lett*. 2015;235:45–59.
32. **Chen Q, Zhang Z, Zhang R, Niu Y, Bian X, Zhang Q.** Tributyltin chloride-induced immunotoxicity and thymocyte apoptosis are related to abnormal Fas expression. *Int J Hyg Environ Health*. 2011; 214:145–150.
33. **Ehrhart-Bornstein M, Hinson JP, Bornstein SR, Scherbaum WA, Vinson GP.** Intraadrenal interactions in the regulation of adrenocortical steroidogenesis. *Endocr Rev*. 1998;19:101–143.
34. **Turrin NP, Rivest S.** Unraveling the molecular details involved in the intimate link between the immune and neuroendocrine systems. *Exp Biol Med (Maywood)*. 2004;229:996–1006.
35. **Incollingo Rodriguez AC, Epel ES, White ML, Standen EC, Seckl JR, Tomiyama AJ.** Hypothalamic-pituitary-adrenal axis dysregulation and cortisol activity in obesity: a systematic review. *Psychoneuroendocrinology*. 2015;62:301–318.
36. **Wester PW, Krajnc EI, van Leeuwen FX, et al.** Chronic toxicity and carcinogenicity of bis(tri-n-butyltin)oxide (TBTO) in the rat. *Food Chem Toxicol*. 1990;28:179–196.
37. **Yamazaki T, Shimodaira M, Kuwahara H, et al.** Tributyltin disturbs bovine adrenal steroidogenesis by two modes of action. *Steroids*. 2005;70:913–921.
38. **Lang Podratz P, Delgado Filho VS, Lopes PF, et al.** Tributyltin impairs the reproductive cycle in female rats. *J Toxicol Environ Health A*. 2012;75:1035–1046.
39. **Rodrigues SM, Ximenes CF, de Batista PR, et al.** Tributyltin contributes in reducing the vascular reactivity to phenylephrine in isolated aortic rings from female rats. *Toxicol Lett*. 2014;225:378–385.
40. **dos Santos RL, Podratz PL, Sena GC, et al.** Tributyltin impairs the coronary vasodilation induced by 17β-estradiol in isolated rat heart. *J Toxicol Environ Health A*. 2012;75:948–959.
41. **Zhou CH, Li ML, Qin AL, et al.** Reduction of fibrosis in dibutyltin dichloride-induced chronic pancreatitis using rat umbilical mesenchymal stem cells from Wharton's jelly. *Pancreas*. 2013;42:1291–1302.
42. **EPA.** *Toxicological Review: Tributyltin Oxide (CAS No 56-35-9) in Support of Summary Information on the Integrated Risk Information System (IRIS)*. Washington, DC: United States Environmental Protection Agency; 1997.
43. **Xia LP, Shen L, Kou H, et al.** Prenatal ethanol exposure enhances the susceptibility to metabolic syndrome in offspring rats by HPA axis-associated neuroendocrine metabolic programming. *Toxicol Lett*. 2014;226:98–105.
44. **Pereiro N, Moyano R, Blanco A, Lafuente A.** Regulation of corticosterone secretion is modified by PFOS exposure at different levels of the hypothalamic-pituitary-adrenal axis in adult male rats. *Toxicol Lett*. 2014;230:252–262.
45. **Domenici Lombardo L, Cortesini C.** The zona glomerulosa of the adrenal gland in rats with portacaval shunt. An ultrastructural and morphometric study. *Int J Exp Pathol*. 1990;71:639–646.
46. **Barcelos LS, Talvani A, Teixeira AS, et al.** Impaired inflammatory angiogenesis, but not leukocyte influx, in mice lacking TNFR1. *J Leukoc Biol*. 2005;78:352–358.
47. **Araujo FA, Rocha MA, Mendes JB, Andrade SP.** Atorvastatin inhibits inflammatory angiogenesis in mice through down regulation of VEGF, TNF-α and TGF-β1. *Biomed Pharmacother*. 2010;64: 29–34.
48. **Quennell JH, Howell CS, Roa J, Augustine RA, Grattan DR, Anderson GM.** Leptin deficiency and diet-induced obesity reduce hypothalamic kisspeptin expression in mice. *Endocrinology*. 2011; 152:1541–1550.
49. **Livak KJ, Schmittgen TD.** Analysis of relative gene expression data using real-time quantitative PCR and the $2(-\Delta\Delta C(T))$ method. *Methods*. 2001;25:402–408.
50. **Vahl TP, Ulrich-Lai YM, Ostrander MM, et al.** Comparative analysis of ACTH and corticosterone sampling methods in rats. *Am J Physiol Endocrinol Metab*. 2005;289:823–828.
51. **Liu L, Mu Y, Han W, Wang C.** Association of hypercholesterolemia and cardiac function evaluated by speckle tracking echocardiography in arabbit model. *Lipids Health Dis*. 2014;13:128.
52. **Felszeghy K, Bagdy G, Nyakas C.** Blunted pituitary-adrenocortical stress response in adult rats following neonatal dexamethasone treatment. *J Neuroendocrinol*. 2000;12:1014–1121.
53. **Spanswick SC, Epp JR, Sutherland RJ.** Time-course of hippocampal granule cell degeneration and changes in adult neurogenesis after adrenalectomy in rats. *Neuroscience*. 2011;190:166–176.
54. **Funahashi N, Iwasaki I, Ide G.** Effects of bis (tri-n-butyltin) oxide on endocrine and lymphoid organs of male rats. *Acta Pathol Jpn*. 1980;30:955–966.
55. **Krajnc EI, Wester PW, Loeber JG, et al.** Toxicity of bis(tri-n-butyltin)oxide in the rat. I. Short-term effects on general parameters and on the endocrine and lymphoid systems. *Toxicol Appl Pharmacol*. 1984;30:363–386.
56. **Morita Y, Yanagida D, Shintani N, et al.** Lack of trimethyltin (TMT)-induced elevation of plasma corticosterone in PACAP-deficient mice. *Ann NY Acad Sci*. 2006;1070:450–456.
57. **Weger BD, Weger M, Nusser M, Brenner-Weiss G, Dickmeis T.** A chemical screening system for glucocorticoid stress hormone signaling in an intact vertebrate. *ACS Chem Biol*. 2012;7:1178–1183.
58. **Baes M, Allaerts W, Denef C.** Evidence for functional communication between folliculostellate cells and hormone secreting cells in perifused anterior pituitary cell aggregates. *Endocrinology*. 1987; 120:685–691.
59. **Allaerts W, Carmeliet P, Denef C.** New perspectives in the function of pituitary folliculostellate cells. *Mol Cell Endocrinol*. 1990;71: 73–81.
60. **Vidal S, Rotondo F, Horvath E, Kovacs K, Scheithauer BW.** Immunocytochemical localization of mast cells in lymphocytic hypophysitis. *Am J Clin Pathol*. 2002;117:478–483.
61. **Rotondo F, Quintanar-Stephano A, Asa SL, et al.** Adenohypophysitis in rat pituitary allografts. *Int J Exp Pathol*. 2010;91:445–450.
62. **Gordon JR, Burd PR, Galli SJ.** Mast cells as a source of multifunctional cytokines. *Immunol Today*. 1990;11:458–464.
63. **Arzt E, Pereda MP, Castro CP, Pagotto U, Renner U, Stalla GK.** Pathophysiological role of the cytokine network in the anterior pituitary gland. *Front Neuroendocrinol*. 1999;20:71–95.
64. **Iuchi T, Saeki N, Tanaka M, Sunami K, Yamaura A.** MRI prediction of fibrous pituitary adenomas. *Acta Neurochir (Wien)*. 1998; 140:779–786.
65. **Naganuma H, Satoh E, Nukui H.** Technical considerations of transsphenoidal removal of fibrous pituitary adenomas and evaluation of collagen contente and subtype in the adenomas. *Neurol Med Chir (Tokyo)*. 2002;42:202–212.
66. **Calogero AE, Gallucci WT, Gold PW, Chrousos GP.** Multiple feedback regulatory loops upon rat hypothalamic corticotropin-releasing hormone secretion. Potential clinical implications. *J Clin Invest*. 1988;82:767–774.
67. **Aguilera G.** HPA axis responsiveness to stress: implications for healthy aging. *Exp Gerontol*. 2011;46:90–95.
68. **Zhang C, Xu D, Luo H, et al.** Prenatal xenobiotic exposure and intrauterine hypothalamus-pituitary-adrenal axis programming alteration. *Toxicology*. 2014;325:74–84.
69. **Chen F, Zhou L, Bai Y, Zhou R, Chen L.** Sex differences in the adult HPA axis and affective behaviors are altered by perinatal exposure to a low dose of bisphenol A. *Brain Res*. 2014;1571:12–24.

70. **Maric NP, Adzic M.** Pharmacological modulation of HPA axis in depression–new avenues for potential therapeutic benefits. *Psychiatr Danub*. 2013;25:299–305.
71. **Bornstein SR, Engeland WC, Ehrhart-Bornstein M, Herman JP.** Dissociation of ACTH and glucocorticoids. *Trends Endocrinol Metab*. 2008;19:175–180.
72. **Gaillard RC, Turnill D, Sappino P, Muller AF.** Tumor necrosis factor α inhibits the hormonal response of the pituitary gland to hypothalamic releasing factors. *Endocrinology*. 1990;127:101–106.
73. **Vankelecom H, Carmeliet P, Heremans H, et al.** Interferon-γ inhibits stimulated adrenocorticotropin, prolactin, and growth hormone secretion in normal rat anterior pituitary cell cultures. *Endocrinology*. 1990;126:2919–2926.
74. **Polito A, Sonneville R, Guidoux C, et al.** Changes in CRH and ACTH synthesis during experimental and human septic shock. *PLoS One*. 2011;6:e25905.
75. **Rivier C.** Role of nitric oxide in regulating the rat hypothalamic-pituitary-adrenal axis response to endotoxemia. *Ann NY Acad Sci*. 2003;992:72–85.
76. **Sawchenko PE, Swanson LW.** Localization, colocalization, and plasticity of corticotropin-releasing factor immunoreactivity in rat brain. *Fed Proc*. 1985;44:221–227.
77. **Koob GF, Bloom FE.** Corticotropin-releasing factor and behavior. *Fed Proc*. 1985;44:259–263.
78. **Makino S, Shibasaki T, Yamauchi N, et al.** Psychological stress increased corticotropin-releasing hormone mRNA and content in the central nucleus of the amygdala but not in the hypothalamic paraventricular nucleus in the rat. *Brain Res*. 1999;850:136–143.
79. **Aguilera G, Liu Y.** The molecular physiology of CRH neurons. *Front Neuroendocrinol*. 2012;33:67–84.
80. **Kanczkowski W, Sue M, Zacharowski K, Reincke M, Bornstein SR.** The role of adrenal gland microenvironment in the HPA axis function and dysfunction during sepsis. *Mol Cell Endocrinol*. 2015;408:241–248.
81. **Silverman MN, Pearce BD, Biron CA, Miller AH.** Immune modulation of the hypothalamic-pituitary-adrenal (HPA) axis during viral infection. *Viral Immunol*. 2005;18:41–78.
82. **Prigent H, Maxime V, Annane D.** Science review: mechanisms of impaired adrenal function in sepsis and molecular actions of glucocorticoids. *Crit Care*. 2004;8:243–252.
83. **Stinnett GS, Westphal NJ, Seasholtz AF.** Pituitary CRH-binding protein and stress in female mice. *Physiol Behav*. 2015;150:16–23.
84. **Dhabhar FS, McEwen BS, Spencer RL.** Adaptation to prolonged or repeated stress–comparison between rat strains showing intrinsic differences inreactivity to acute stress. *Neuroendocrinology*. 1997;65:360–368.
85. **Lamounier-Zepter V, Ehrhart-Bornstein M.** Fat tissue metabolism and adrenal steroid secretion. *Curr Hypertens Rep*. 2006;8:30–34.
86. **Saitoh M, Yanase T, Morinaga H, et al.** Tributyltin or triphenyltin inhibits aromatase activity in the human granulosa-like tumor cell line KGN. *Biochem Biophys Res Commun*. 2001;289:198–204.
87. **Mitra S, Srivastava A, Khanna S, Khandelwal S.** Consequences of tributyltin chloride induced stress in Leydig cells: an ex-vivo approach. *Environ Toxicol Pharmacol*. 2014;37:850–860.
88. **Jefcoate C.** High-flux mitochondrial cholesterol trafficking, a specialized function of the adrenal cortex. *J Clin Invest*. 2002;110:881–890.
89. **Clark BJ, Ranganathan V, Combs R.** Steroidogenic acute regulatory protein expression is dependent upon post-translational effects of cAMP-dependent protein kinase A. *Mol Cell Endocrinol*. 2001;173:183–192.
90. **Harvey PW, Everett DJ, Springall CJ.** Adrenal toxicology: a strategy for assessment of functional toxicity to the adrenal cortex and steroidogenesis. *J Appl Toxicol*. 2007;27:103–115.
91. **Milovanović T, Budec M, Balint-Perić L, Koko V, Todorović V.** Effects of acute administration of ethanol on the rat adrenal cortex. *J Stud Alcohol*. 2003;64:662–668.
92. **Schober A, Huber K, Fey J, Unsicker K.** Distinct populations of macrophages in the adult rat adrenal gland: a subpopulation with neurotrophin-4-likeimmunoreactivity. *Cell Tissue Res*. 1998;291:365–373.
93. **Wolkersdörfer GW, Lohmann T, Marx C, et al.** Lymphocytes stimulate dehydroepiandrosterone production through direct cellular contact with adrenal zona reticularis cells: a novel mechanism of immune-endocrine interaction. *J Clin Endocrinol Metab*. 1999;84:4220–4227.
94. **Kim JS, Kubota H, Nam SY, Doi K, Saegusa J.** Expression of cytokines and proteases in mast cells in the lesion of subcapsular cell hyperplasia in mouse adrenal glands. *Toxicol Pathol*. 2000;28:297–303.
95. **Bornstein SR, Chrousos GP.** Clinical review 104: adrenocorticotropin (ACTH)- and non-ACTH-mediated regulation of the adrenal cortex: neural and immune inputs. *J Clin Endocrinol Metab*. 1999;84:1729–1736.
96. **Kanczkowski W, Chatzigeorgiou A, Samus M, et al.** Characterization of the LPS-induced inflammation of the adrenal gland in mice. *Mol Cell Endocrinol*. 2013;371:228–235.
97. **Kim JS, Kubota H, Doi K, Saegusa J.** Correlation of mast cells with spindle cell hyperplasia in the adrenal cortex of IQI/Jic mice. *Exp Anim*. 1997;46:103–109.
98. **Reed CT, Adams K, Shenoy V.** Xanthogranulomatous adrenalitis: a case report of a diabetic, 55-year-old male. *Endocr Pathol*. 2015;26:229–231.
99. **Stocco DM, Clark BJ.** Regulation of the acute production of steroids in steroidogenic cells. *Endocr Rev*. 1996;17:221–244.
100. **Cheng B, Chou SC, Abraham S, Kowal J.** Effects of prolonged ACTH-stimulation on adrenocortical cholesterol reserve and apolipoprotein E concentration in young and aged Fischer 344 male rats. *J Steroid Biochem Molec Biol*. 1998;66:335–345.
101. **Delprado WJ, Baird PJ.** The fetal adrenal gland: lipid distribution with associated intrauterine hypoxia. *Pathology*. 1984;16:25–29.
102. **Szabó D, Tóth IE, Szalay KS.** Viscosity of rat adrenocortical lipids in different functional states: morphological characteristics. *J Steroid Biochem Mol Biol*. 1996;58:329–335.
103. **Miller WL, Strauss JF 3rd.** Molecular pathology and mechanism of action of the steroidogenic acute regulatory protein, StAR. *J Steroid Biochem Mol Biol*. 1999;69:131–141.
104. **Lin D, Sugawara T, Strauss JF 3rd, et al.** Role of steroidogenic acute regulatory protein in adrenal and gonadal steroidogenesis. *Science*. 1995;267:1828–1831.
105. **Kirchner S, Kieu T, Chow C, Casey S, Blumberg B.** Prenatal exposure to the environmental obesogen tributyltin predisposes multipotent stem cells to become adipocytes. *Mol Endocrinol*. 2010;24:526–539.
106. **Zuo Z, Chen S, Wu T, Zhang J, Su Y, Chen Y, Wang C.** Tributyltin causes obesity and hepatic steatosis in male mice. *Environ Toxicol*. 2011;26:79–85.
107. **Tontonoz P, Hu E, Spiegelman BM.** Stimulation of adipogenesis in fibroblasts by PPAR γ2, a lipid-activated transcription factor. *Cell*. 1994;79:1147–1156.
108. **Rosen ED, Walkey CJ, Puigserver P, Spiegelman BM.** Transcriptional regulation of adipogenesis. *Genes Dev*. 2000;14:1293–1307.
109. **Penza M, Jeremic M, Marrazzo E, et al.** The environmental chemical tributyltin chloride (TBT) shows both estrogenic and adipogenic activities in mice which might depend on the exposure dose. *Toxicol Appl Pharmacol*. 2011;255:65–75.
110. **Chamorro-García R, Sahu M, Abbey RJ, Laude J, Pham N, Blumberg B.** Transgenerational inheritance of increased fat depot size, stem cell reprogramming, and hepatic steatosis elicited by prenatal exposure to the obesogen tributyltin in mice. *Environ Health Perspect*. 2013;121:359–366.

111. **Sies H.** Oxidative stress: oxidants and antioxidants. *Exp Physiol*. 1997;82:291–295.
112. **Nordberg J, Arnér ES.** Reactive oxygen species, antioxidants, and the mammalian thioredoxin system. *Free Radic Biol Med*. 2001; 31:1287–1312.
113. **Spiers JG, Chen HJ, Sernia C, Lavidis NA.** Activation of the hypothalamic-pituitary-adrenal stress axis induces cellular oxidative stress. *Front Neurosci*. 2015;8:456.
114. **Mitra S, Siddiqui WA, Khandelwal S.** Differential susceptibility of brain regions to tributyltin chloride toxicity. *Environ Toxicol Pharmacol*. 2014;37:1048–1059.
115. **Annabi A, Dhouib IB, Lamine AJ, et al.** Recovery by N-acetylcysteine from subchronic exposure to Imidacloprid-induced hypothalamic-pituitary-adrenal (HPA) axis tissues injury in male rats. *Toxicol Mech Methods*. 2015;29:1–8.
116. **Kaida S, Ohta Y, Imai Y, Ohashi K, Kawanishi M.** Compound 48/80 causes oxidative stress in the adrenal gland of rats through mast cell degranulation. *Free Radic Res*. 2010;44:171–180.
117. **Brown KA, Brain SD, Pearson JD, Edgeworth JD, Lewis SM, Treacher DF.** Neutrophils in development of multiple organ failure in sepsis. *Lancet*. 2006;368:157–169.
118. **Buttke TM, Sandstrom PA.** Oxidative stress as a mediator of apoptosis. *Immunol Today*. 1994;15:7–10.
119. **Chandra J, Samali A, Orrenius S.** Triggering and modulation of apoptosis by oxidative stress. *Free Radic Biol Med*. 2000;29:323–333.
120. **Haddad JJ.** Redox and oxidant-mediated regulation of apoptosis signaling pathways: immuno-pharmaco-redox conception of oxidative siege versus cell death commitment. *Int Immunopharmacol*. 2004;4:475–493.
121. **Stridh H, Kimland M, Jones DP, Orrenius S, Hampton MB.** Cytochrome c release and caspase activation in hydrogen peroxide and tributyltin-induced apoptosis. *FEBS Lett*. 1999;8429:351–355.
122. **Gennari A, Viviani B, Galli CL, Marinovich M, Pieters R, Corsini E.** Organotins induce apoptosis by disturbance of $[Ca^{2+}]i$ and mitochondrial activity, causing oxidative stress and activation of caspases in rat thymocytes. *Toxicol Appl Pharmacol*. 2000;169: 185–190.
123. **Nakatsu Y, Kotake Y, Ohta S.** Concentration dependence of the mechanisms of tributyltin-induced apoptosis. *Toxicol Sci*. 2007; 97:438–447.
124. **Shao C, Yu L, Gao L.** Activation of angiotensin type 2 receptors partially ameliorates streptozotocin-induced diabetes in male rats by islet protection. *Endocrinology*. 2014;155:793–804.
125. **Osamura RY, Watanabe K, Oh M.** Melanin-containing cells in the uterine cervix: histochemical and electron-microscopic studies of two cases. *Am J Clin Pathol*. 1980;74:239–242.
126. **He P, Chen Z, Sun Q, Li Y, Gu H, Ni X.** Reduced expression of 11β-hydroxysteroid dehydrogenase type 2 in preeclamptic placentas is associated with decreased PPARγ but increased PPARα expression. *Endocrinology*. 2014;155:299–309.
127. **Yao W, Yu X, Fang Z, et al.** Profilin1 facilitates staurosporine-triggered apoptosis by stabilizing the integrin β1-actin complex in breast cancer cells. *J Cell Mol Med*. 2012;16:824–835.
128. **Heneka MT, Klockgether T, Feinstein DL.** Peroxisome proliferator-activated receptor-gamma ligands reduce neuronal inducible nitric oxide synthase expression and cell death in vivo. *J Neurosci*. 2000;20:6862–6867.
129. **García-Corzo L, Luna-Sánchez M, Doerrier C, et al.** Dysfunctional Coq9 protein causes predominant encephalomyopathy associated with CoQ deficiency. *Hum Mol Genet*. 2013;22:1233–1248.